

# We are IntechOpen, the world's leading publisher of Open Access books Built by scientists, for scientists

6,900

Open access books available

185,000

International authors and editors

200M

Downloads

Our authors are among the

154

Countries delivered to

TOP 1%

most cited scientists

12.2%

Contributors from top 500 universities



WEB OF SCIENCE™

Selection of our books indexed in the Book Citation Index  
in Web of Science™ Core Collection (BKCI)

Interested in publishing with us?  
Contact [book.department@intechopen.com](mailto:book.department@intechopen.com)

Numbers displayed above are based on latest data collected.  
For more information visit [www.intechopen.com](http://www.intechopen.com)



---

# Microwave Dielectrics with Perovskite-Type Structure

---

Hitoshi Ohsato

Additional information is available at the end of the chapter

<http://dx.doi.org/10.5772/61718>

---

## Abstract

Most electroceramics are ferroelectrics, but microwave dielectrics are mostly paraelectrics with a center of symmetry  $i$ . Microwave dielectrics should possess a perfect crystal structure with neither defects nor internal strain in order to be microwave friendly. They have been used in resonators and filters in mobile telecommunications devices. Perovskite and related compounds are also mostly ferroelectrics, but paraelectrics with a perovskite structure also exist, and are used in microwave dielectrics. Owing to the flexibility of the perovskite structure, many kinds of microwave dielectrics with a perovskite structure have been designed for microwave dielectrics. In this chapter, simple and complex perovskite, and perovskite related materials such as pseudo-tungsten-bronze solid solutions and homologous compounds are introduced for microwave dielectrics. The microwave dielectric properties are revealed through the crystalline structure of the material. Therefore, the relationship between the crystalline structure and properties of the material is presented, and is expected to be of use in the design of novel dielectrics. As many superior materials for microwave dielectrics have been developed and are expected to be used in new applications such as wireless sensors and wireless power transfer by resonant coupling, wave absorption by interference and transparent ceramics with no birefringence, these new applications are also discussed.

**Keywords:** Microwave dielectrics, Complex Perovskite, Ordering, Tungsten-bronze compounds, Homologous series

---

## 1. Introduction

Perovskite and related compounds are the main materials used in microwave dielectrics, as shown in Fig. 1. The data are listed in a database proposed by M. T. Sebastian and published in the book “*Dielectric materials for wireless communication*” [1]. The book cites about 2,300 compounds with about 750 references making it an excellent publication for material scientists and researchers, particularly with respect to microwave technology. The data for dielectric

materials is now being updated with about 3,000 compounds and 1,600 references which has now been published [2]. A sizeable amount (about 46%) includes rare-earth (*R*) ions with colors as shown in Fig. 2(a), and these were reviewed in a chapter of the book [3] and various papers [4, 5]. The largest amount of compounds (45%) are of the perovskite-type, known as the 'King' of electroceramics, and the second largest group of compounds, at 21%, are the pseudo-tungsten-bronze solid solutions, also related to perovskite compounds, as shown in Fig. 1.

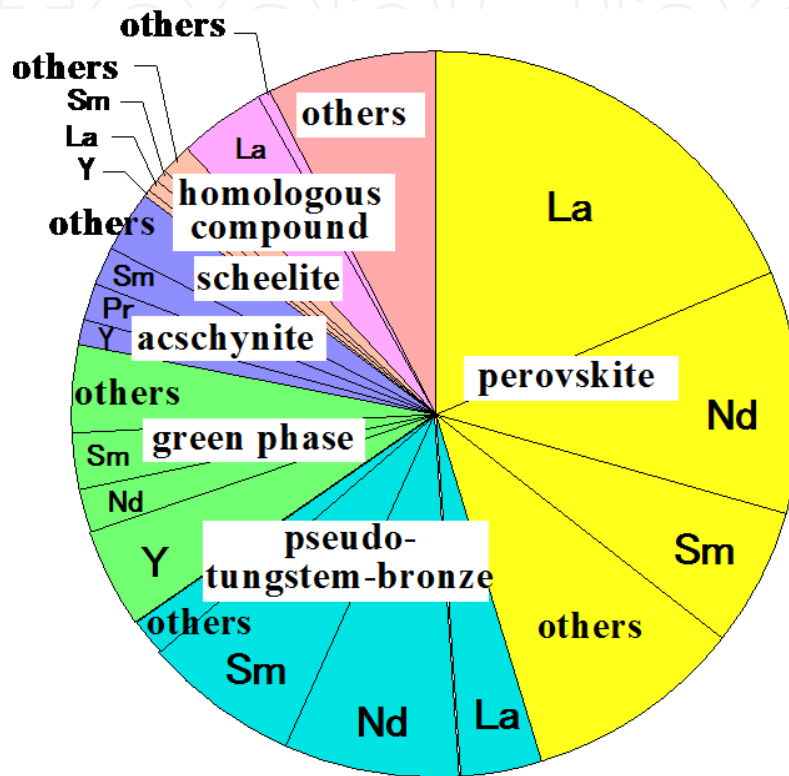


Figure 1. Ratio of microwave dielectric compounds with different crystal structures.



Figure 2. (a) Dielectric resonators. (b) LTCC for LC filter. (NTK/NGK)

Microwave dielectrics have been used as a key constituent of wireless communications [6–9]. Microwave dielectrics are used in resonators, filters and temperature stable capacitors with a near zero temperature coefficient of resonant frequency ( $TC_f$ ) / temperature coefficient of

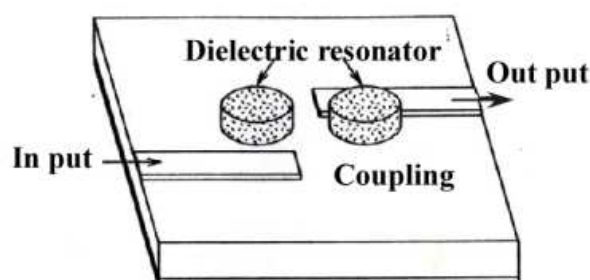


Figure 3. Dielectric resonator with resonant coupling.

dielectric constant ( $TC\epsilon_r$ ) and so on (Fig. 3). Originally, microwave dielectrics were developed from the temperature stable capacitor which shows a near zero  $TC\epsilon_r$  as explained in section 2. Resonators and filters are used in mobile communication technology. In the early days of information technology (IT), microwave dielectrics replaced cavity resonators and worked extremely well in reducing the size of the equipment used — from the car telephone to the shoulder phone by 1987 for example. Moreover, microwave dielectrics have been developed for a wide range of telecommunication applications, such as mobile phones, wireless LAN, and intelligent transport system (ITS). Fig. 4 shows three directions of development of microwave dielectrics, which presented  $Q \cdot f$  as a function of the dielectric constant  $\epsilon_r$  [10]. The curve in the figure shows the outline of the upper limit of  $Q \cdot f$  obtained for a given  $\epsilon_r$ . The first direction with a high  $\epsilon_r$  is mainly used in the miniaturization of mobile phone components. The second one, with a high  $Q$  and a high  $\epsilon_r$  is in demand for use in mobile phone base stations. The third direction, with a high  $Q$  and a low  $\epsilon_r$  is for devices working in the millimeter-wave range — the new frontiers of microwave dielectrics because the utilizable frequency region is expanding towards the millimeter-wave due to a shortage of conventional radio frequency (RF) regions. The three important microwave dielectric properties of  $\epsilon_r$ ,  $Q \cdot f$  and  $TCf$  are explained in section 2.

These compounds are friendly with electromagnetic waves. When irradiated with an electromagnetic wave, the materials should be resonating owing to dielectric polarization changing under an alternating electromagnetic field as shown in Fig. 5(a). The direction of the dielectric polarization should be easily changeable to the opposite direction depending on the electric field. If the material has spontaneous polarization as in ferroelectrics, then inversion losses become large. As a result most microwave dielectrics are paraelectrics with a center of symmetry  $i$ . The structure of perovskite is flexible, and as a result perovskite shows many kinds of structure, such as cubic, tetragonal, orthorhombic, trigonal, and monoclinic, depending on the particular  $A$  and  $B$  cations in  $ABO_3$ . The author recommends referring to some reports written by the author himself [11-16].

Microwave dielectrics have been studied for more than a half of a century now. Many materials with suitable properties have been identified and should be used in new applications to develop new technologies to aid the survival of humans on the Earth. The next generation of functional advances in microwave dielectrics are presented in a chapter of the “Handbook of Multifunctional Ceramics” [17].

In this chapter, perovskite and related materials used in microwave dielectrics are presented and the relationships between the crystal structure and the properties of the materials are discussed. Moreover, new applications for microwave dielectrics developed up to date are also presented.

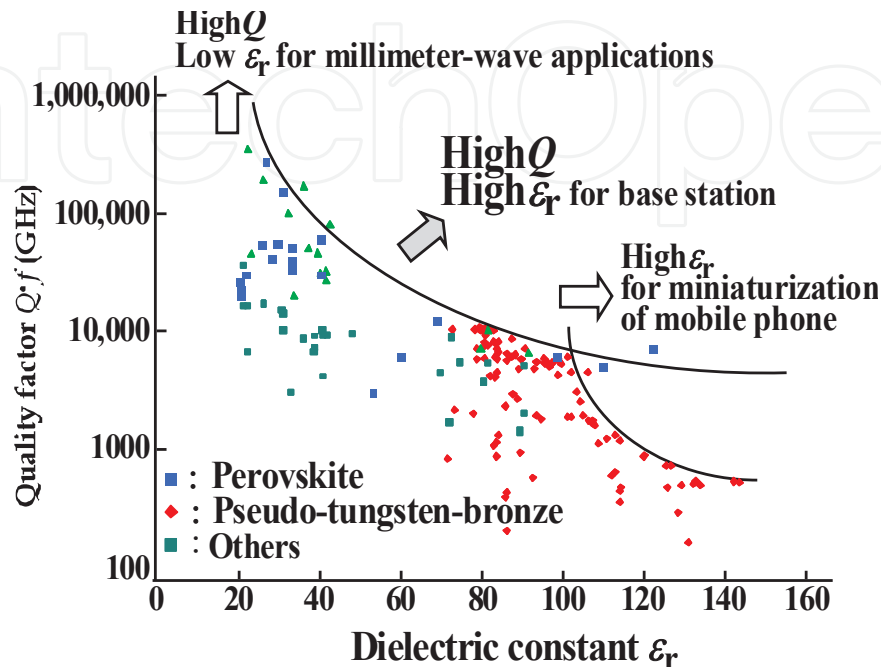


**Figure 4.** Three directions of R&D for microwave dielectrics. The  $Q \cdot f$  of microwave dielectrics is shown as a function of  $\epsilon_r$ .

## 2. Three important microwave dielectric properties

There are three important properties of microwave dielectrics: the quality factor  $Q$ , the dielectric constants  $\epsilon_r$ , and the temperature coefficient of resonant frequency  $TCf$  [18].

### 2.1. Quality factor

Firstly, dielectric materials placed in an electromagnetic field should resonate easily with the electromagnetic waves. In other words, they should have a high quality factor. The quality factor  $Q$  is the inverse of the dielectric loss ( $\tan\delta$ ) and is presented as follows:

$$Q = 1/\tan\delta$$

However, upon measurement, it is usual to obtain a so-called unloaded quality factor  $Q_u$ . This is the sum of the reciprocals of the other factors and depends on the dielectric loss of the materials  $Q_d$ , conduction loss  $Q_c$ , and radiation loss  $Q_r$ .

$$1/Q_u = 1/Q_d + 1/Q_c + 1/Q_r$$

The losses are generated by dielectric polarization in the presence of an electromagnetic wave. Ferroelectric materials with spontaneous polarization have large dielectric losses because of the large movement of cations. So, paraelectric materials with a center of symmetry *i* are suitable for microwave and millimeter-wave dielectrics. Dielectric loss increases with an increase in frequency as shown in Fig. 5 (b). In the case of ultra-high frequencies, the number of polarity changes increases with frequency. Therefore, dielectric materials with a high *Q* value are desirable.

## 2.2. Dielectric constant $\epsilon_r$

The dielectric constant  $\epsilon_r$  causes a shortening of wave length  $\lambda$  in dielectrics as shown in Fig. 5(c) according to the following equation:

$$\lambda = \lambda_0 / \sqrt{\epsilon_r}$$

Here,  $\lambda_0$  is the wave length in a vacuum. In the microwave region, the  $\epsilon_r$  value is expected to be large for the miniaturization of mobile communication equipment. In the millimeter-wave region, the  $\epsilon_r$  value is expected to be small. As the wave length is in the millimeter order, miniaturization is not needed.

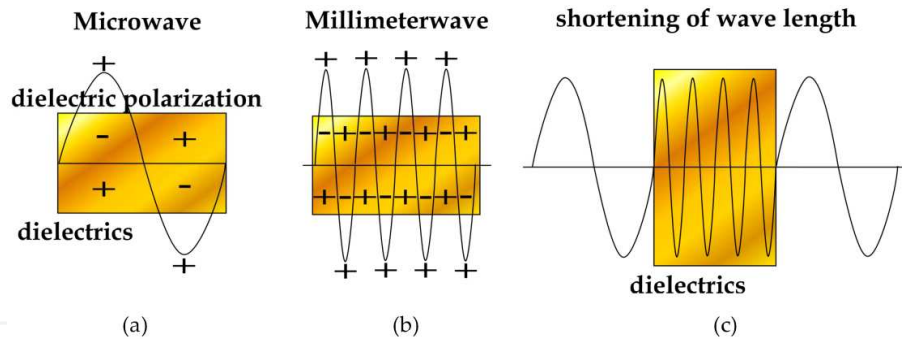


**Figure 5.** (a) When irradiated by electromagnetic waves, the materials should resonate due to changing dielectric polarization under alternating electromagnetic fields. (b) Dielectric losses increase with an increase in frequency. (c)  $\epsilon_r$  causes a shortening of wavelength  $\lambda$  in dielectrics.

There are other more important phenomena such as the time delay  $T_{PD}$  according to the following equation:

$$T_{PD} = \sqrt{\epsilon_r} / c$$

Here,  $\epsilon_r$  is the dielectric constant and *c* is the velocity of light. The time delay is desirable in order to improve the speed of the signal.

The origin of  $\epsilon_r$  was considered by difference of crystal structure as shown in Fig. 6 [19]. Silicates with a low  $\epsilon_r$  are formed by the tetrahedral framework of  $\text{SiO}_4$ , with 45% ionic bonds and 55% covalent bonds. Covalent bonds reduce  $\epsilon_r$ , because the rattling effect of the cations in a polyhedron should be reduced as a result of the high bond strength. On the other hand, titanates (Fig. 6(c)) with a large  $\epsilon_r$  such as  $\text{SrTiO}_3$ , are formed by a  $\text{TiO}_6$  octahedral framework, which is almost of ionic bond and has space for ionic displacement. In the case of aluminates, although Al ions also occupy an octahedral framework, the Al ions located in the paired octahedral on the threefold axis repulse each other as shown in Fig. 6(b). The Al ions are immovable in the octahedron and produce a medium  $\epsilon_r$ . The order of  $\epsilon_r$  is as follows:

$$\epsilon_{r \text{ silicate}} < \epsilon_{r \text{ aluminate}} < \epsilon_{r \text{ titanate}}$$

Silicates with a low  $\epsilon_r$  are good candidates for millimeter-wave dielectrics [19].

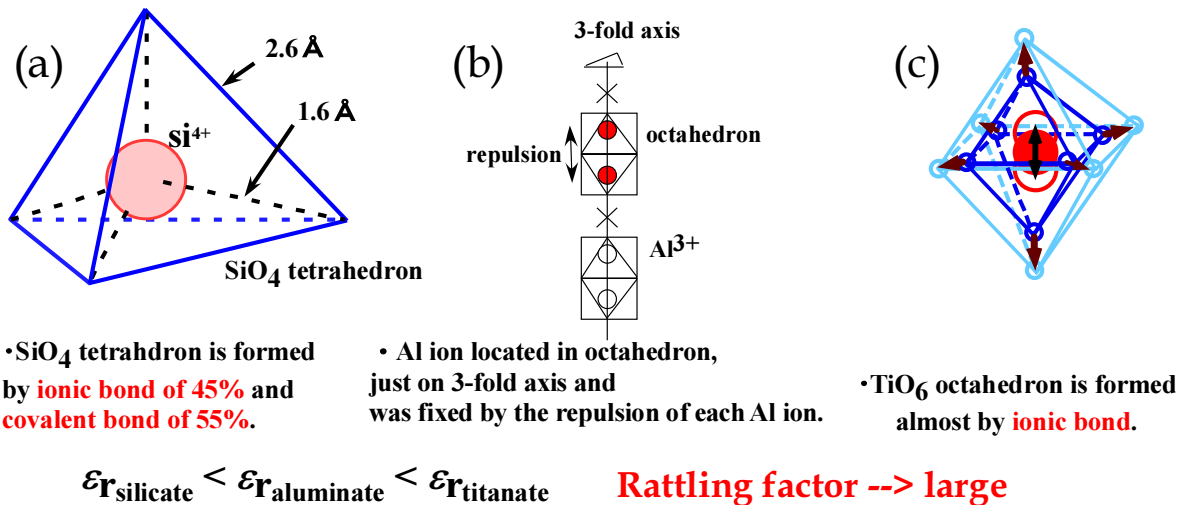


Figure 6. Dielectric constants due to crystal structure: (a)  $\text{SiO}_4$  tetrahedron, (b)  $\text{Al}_2\text{O}_3$  and (c)  $\text{TiO}_6$  octahedron.

### 2.3. Temperature coefficient of resonant frequency $TCf$

The  $TCf$  is required to be near 0 ppm/°C for global usage in different environmental temperatures. The  $TCf$  has a relationship with the temperature coefficient of dielectric constant  $TC\epsilon_r$  as follows:

$$TCf = - (\alpha + TC\epsilon_r/2).$$

Where  $\alpha$  is the thermal expansion coefficient.

Most millimeter-wave compounds with a low  $\epsilon_r$  have a large negative  $TCf$  such as alumina: -65, and forsterite: -70 ppm/°C. The  $TCf$  of these millimeter-wave dielectrics was improved by

two different methods. The first requires the addition of materials with the opposite charge (*i.e.* a positive  $TCf$ ). The addition of rutile with a  $TCf = +450 \text{ ppm}/^\circ\text{C}$  can adjust the  $TCf$  of the compound in question [20–23]. The second method is to adjust the  $TCf$  to near  $0 \text{ ppm}/^\circ\text{C}$  by the formation of the solid solution phases [24]. This is the preferred method because of the small degradation of  $Q \cdot f$ .

### 3. Specialized study

#### 3.1. Perovskite-type compounds

##### 3.1.1. Simple perovskite

Although perovskite compounds commonly used in ferroelectrics shouldn't be used for microwave dielectrics as described in the previous section, perovskite compounds can be flexibly applied to microwave dielectrics. This flexibility is due to the depth of the crystal structure. Table 1 shows the polymorphism of  $\text{BaTiO}_3$  — a representative perovskite-type structure. At room temperature, it is stable due to the tetragonal system, but is ferroelectric without a center of symmetry  $i$ . It transforms to a cubic structure with paraelectricity above a Curie point of  $120^\circ\text{C}$ . In the near future, if devices capable of operating under temperatures of more than  $120^\circ\text{C}$  appear, then it may be applied to microwave devices. At low temperatures, all structures of  $\text{BaTiO}_3$  are ferroelectrics without  $i$ .

Crystal system	Stable temperature region	Space group	Center of symmetry	Lattice parameters Å
Hexagonal	Above $1460^\circ\text{C}$	$P6_3/mmc$ (No.194)	$i$	$a = 5.72481$ $c = 13.9673$
Cubic	$120 \sim 1460^\circ\text{C}$	$Pm\bar{3}m$ (No.221)	$i$	$a = 4.038$
Tetragonal	$5 \sim 120^\circ\text{C}$	$P4mm$ (No.99)	non	$a = 3.994$ $c = 4.038$
Orthorhombic	$-90 \sim 5^\circ\text{C}$	$Amm2$ (No.38)	non	$a = 3.990$ $b = 5.669$ $c = 5.682$
Trigonal (Rhombohedral)	Under $-90^\circ\text{C}$	$R3m$ (No.160)	non	$a = 5.6560$ $c = 6.9509$ $(a = 4.004,$ $\alpha = 89.870^\circ)$

**Table 1.** Crystal data for  $\text{BaTiO}_3$

Currently, microwave dielectrics of perovskite-type and related compounds are detailed in the database created by Sebastian [1, 2]. Some simple perovskite-type compounds are  $\text{ATiO}_3$ ,

$AZrO_3$  ( $A^{2+} = Ba, Sr$  and  $Ca$ ) and  $RBO_3$  ( $R^{3+} = \text{rare earth}, B^{3+} = Al, Ga$ ).  $MgTiO_3$  and  $ZnTiO_3$  with their small ionic cations of  $Mg$  and  $Zn$  are not perovskite-type structures, but are of the ilmenite-type similar to the structure of  $Al_2O_3$  with oxygen closest packing structure. Table 2(a) shows three microwave properties of simple perovskite-type compounds. These have different crystal structures such as cubic, orthorhombic and hexagonal, but qualify as microwave dielectrics because they have a center of symmetry  $i$ .  $SrTiO_3$  has the crystal structure closest to  $BaTiO_3$ . It is expected to be a microwave dielectric due to the cubic structure of the paraelectric at room temperature. However, one disadvantageous point is that the temperature coefficient of resonant frequency  $TCf$  is too large at 1,200 ppm/°C.  $CaTiO_3$  with the mineral name “perovskite” is orthorhombic in the space group  $Pnma$  (No.62) with  $i$  [25]. The characteristic structure of  $CaTiO_3$  is a tilting octahedral. This compound also has a large  $TCf$  of over 859 ppm/°C, so it could not be used by itself as a microwave dielectrics. Nonetheless, this compound has been used as a stabilizer of  $TCf$  against microwave compounds with a negative  $TCf$ , as most useful microwave dielectrics have a positive  $TCf$ .  $MgTiO_3$  with  $TCf = -45$  ppm/°C was improved to a near zero  $TCf$  by adding  $CaTiO_3$ . This compound with  $\epsilon_r = 21$  and  $Q \cdot f = 8,000$  GHz was the first one used in practice in microwave dielectrics. Recently, in an ilmenite system, a Co doped  $MgTiO_3$  dielectric with a high  $Q \cdot f$  (864,000 GHz) was found, and its  $TCf$  was improved to near zero by the addition of  $CaTiO_3$  [28].

(a) Simple perovskite			
Compound	$\epsilon_r$	$Q \cdot f (10^3 \cdot \text{GHz})$	$TCf (\text{ppm}/^\circ\text{C})$
$SrTiO_3$	304	3.3	1700
$CaTiO_3$	162	12.96	859
$BaZrO_3$	35	8.8	-
$SrZrO_3$	30	13.6	-60
$CaZrO_3$	30	26.4	-27
$NdGaO_3$	22	85	-
$LaAlO_3$	23.4	68	-44
$SmAlO_3$	20.4	65	-74
$NdAlO_3$	22.3	58	-33
$YAlO_3$	15.7	58	-59
$PrAlO_3$	23.2	51	-25
(b) Modified simple perovskite			
$0.2SrTiO_3 \cdot 0.8LaAlO_3$	26.7	139	-50
$0.64CaTiO_3 \cdot 0.34LaGaO_3$	46.5	48	-2.9
$0.7CaTiO_3 \cdot 0.3NdAlO_3$	43	47	0
$0.35CaTiO_3 \cdot 0.65LaAlO_3$	37	47	-2

$0.7\text{CaTiO}_3 \cdot 0.3\text{SmAlO}_3$	45	42	1
$0.7\text{CaTiO}_3 \cdot 0.3(\text{La}_{1/2}\text{Nd}_{1/2})(\text{Ga}_{1/2}\text{Al}_{1/2})\text{O}_3$	45.2	43	9.3
$\text{NdAlO}_3 + 0.25 \text{ wt}\% \text{V}_2\text{O}_5$	21.5	64	-30
$\text{NdAlO}_3 + 0.25 \text{ wt}\% \text{CuO}$	22.4	63	-35
$\text{LaAlO}_3 + 0.25 \text{ wt}\% \text{CuO}$	20.7	48	-80
$0.95(\text{Mg}_{0.95}\text{Co}_{0.05})\text{TiO}_3 \cdot 0.05\text{CaTiO}_3$	20.3	107	-22.8
$0.91(\text{MgZn})_2\text{TiO}_4 \cdot 0.09\text{CaTiO}_3$	22.5	86	3
$0.94\text{MgTiO}_3 \cdot 0.36\text{SrTiO}_3$	20.8	71	-1
$0.95\text{MgTiO}_3 \cdot 0.05\text{CaTiO}_3$	21	56	0
(c) 1:2 type complex perovskite			
$\text{Ba}_{0.9925}(\text{Mg}_{0.033}\text{Ta}_{0.67})\text{O}_3$	24.7	152	1.2
$\text{Ba}(\text{Mg}_{0.3183}\text{Ta}_{0.67})\text{O}_3$	25.1	120.5	3.3
$\text{Ba}(\text{Mg}_{1/3}\text{Ta}_{2/3})\text{O}_3$	24	100.5	8
$\text{Ca}(\text{Mg}_{1/3}\text{Ta}_{2/3})\text{O}_3$	21	78	-61
$\text{Sr}(\text{Mg}_{1/3}\text{Ta}_{2/3})\text{O}_3$	22	5.6	-50
$\text{Ba}(\text{Zn}_{1/3}\text{Ta}_{2/3})\text{O}_3$	30	135	2
$\text{Sr}(\text{Zn}_{1/3}\text{Ta}_{2/3})\text{O}_3$	28	55	-62
$\text{Ca}(\text{Zn}_{1/3}\text{Ta}_{2/3})\text{O}_3$	25	25	-66
$\text{Ba}(\text{Zn}_{1/3}\text{Nb}_{2/3})\text{O}_3$	41.1	86.9	31
$\text{Ba}(\text{Mn}_{1/3}\text{Ta}_{2/3})\text{O}_3$	32	58.2	34
$\text{La}(\text{Mg}_{2/3}\text{Ta}_{1/3})\text{O}_3$	24.7	65.5	-65
(d) 1:1 type complex perovskite			
$\text{Ba}(\text{Mg}_{1/2}\text{W}_{1/2})\text{O}_3$	19	100	-34
$\text{Ca}(\text{Ga}_{1/2}\text{Ta}_{1/2})\text{O}_3$	25	100	-81
$\text{Sr}(\text{Ga}_{1/2}\text{Ta}_{1/2})\text{O}_3$	27	91	-51
$\text{Sr}(\text{Sm}_{1/2}\text{Ta}_{1/2})\text{O}_3$	27.7	59	-63
$\text{La}(\text{Mg}_{1/2}\text{Ti}_{1/2})\text{O}_3$	27.6	114.3	-81
$\text{Sm}(\text{Co}_{1/2}\text{Ti}_{1/2})\text{O}_3$	25.5	76	-16
$\text{La}(\text{Co}_{1/2}\text{Ti}_{1/2})\text{O}_3$	30	67	-64
(e) Solid solutions of 1:2 and 1:1 types of complex perovskite			
$\text{Ba}(\text{Mg}_{1/2}\text{Ta}_{2/3})\text{O}_3 : 0.5 \text{ mol}\% \text{Ba}(\text{Mg}_{1/2}\text{W}_{1/2})\text{O}_3$	24.2	400	-
$0.95\text{Ba}(\text{Zn}_{1/2}\text{Ta}_{2/3})\text{O}_3 \cdot 0.05(\text{Sr}_{1/4}\text{Ba}_{3/4})(\text{Ga}_{1/2}\text{Ta}_{1/2})\text{O}_3$	31	210	-

$0.7\text{Ba}(\text{Mg}_{1/3}\text{Ta}_{2/3})\text{O}_3 \cdot 0.3\text{Ba}(\text{Co}_{1/3}\text{Nb}_{2/3})\text{O}_3$	27	165	-1.3
$\text{Ba}(\text{ZnTa})\text{O}_3 \cdot \text{Ba}(\text{ZnNb})\text{O}_3$	30	164	0
$\text{Ba}(\text{Mg}_{1/3}\text{Ta}_{2/3})\text{O}_3 \cdot \text{Ba}(\text{Zn}_{1/3}\text{Ta}_{2/3})\text{O}_3$	27	150	0
$0.5\text{Ba}(\text{MgTa})\text{O}_3 \cdot 0.5\text{Ba}(\text{ZnTa})\text{O}_3$	27	135	1.95
$0.95\text{Ba}(\text{Zn}_{1/3}\text{Nb}_{2/3})\text{O}_3 \cdot 0.05\text{Ba}(\text{Ga}_{1/2}\text{Ta}_{1/2})\text{O}_3$	38	102.96	19
$\text{Ba}(\text{Ni}_{1/3}\text{Ta}_{2/3})\text{O}_3 \cdot \text{Ba}(\text{ZrZnTa})\text{O}_3$	30	100	0
(f) Modified complex perovskite			
$\text{Ba}(\text{Mg}_{1/3}\text{Ta}_{2/3})\text{O}_3 \cdot \text{BaSnO}_3, \text{BaWO}_4$	24	430	5
$\text{Ba}[(\text{Zn}_{0.6}\text{Co}_{0.4})_{1/3}\text{Nb}_{2/3}]\text{O}_3$	35.6	351.95	-
$\text{Ba}[(\text{Mg}_{1-x}\text{Zn}_x)_{1/3}\text{Ta}_{2/3}]\text{O}_3$	24-26	200-300	-0.5-1.7
$\text{Ba}(\text{Zn}_{1/3}\text{Ta}_{2/3})\text{O}_3$ ; Ga, Zr	30	165.4	0
$\text{Ba}(\text{SnMgTa})\text{O}_3$	24.2	120	-
$\text{Ba}[(\text{Mg}_{0.4}\text{Zn}_{0.6})\text{Ta}_{2/3}]\text{O}_3$	27.7	109.9	6.3
$\text{Ba}(\text{Zr}_{0.05}\text{Zn}_{0.32}\text{Ta}_{0.63})\text{O}_3$	30.4	105	8
$\text{Ba}(\text{M}_{0.33}\text{Ta}_{0.63}\text{Ti}_{0.017}\text{W}_{0.017})\text{O}_3$	24.5	100.7	12.6
$\text{Ba}(\text{Mg}_{0.30}\text{Ta}_{0.60}\text{Ti}_{0.10})\text{O}_3$	26.3	100	14.4
$(\text{Ba}_{1-z}\text{Sr}_z)[\text{Zn}_{1/3}(\text{Ta}_p\text{Nb}_{1-p})_{2/3}](\text{Sr}_{1-x}\text{Ca}_x)(\text{Ga}_{1/2}\text{Ta}_{1/2})\text{O}_3$	32-34	180-80	0-10
$\text{Ba}(\text{SnMgTa})\text{O}_3$	24.2	120	-
(g) Pseudo-tungsten-bronze solid solutions ( $x$ : $\text{Ba}_{6-3x}\text{R}_{8+2x}\text{Ti}_{18}\text{O}_{54}$ , R: Rare earth)			
$\text{Ba}_4\text{Sm}_{9.33}\text{Ti}_{18}\text{O}_{54}$ ( $x=2/3$ )	80	10.7	-15
$\text{Ba}_4\text{Nd}_{9.33}\text{Ti}_{18}\text{O}_{54}$ ( $x=2/3$ )	82.5	10.1	71.1
$\text{Ba}_4\text{Sm}_{8.33}\text{EuTi}_{18}\text{O}_{54}$ ( $x=2/3$ )	78.7	9.56	-10.5
$\text{Ba}_4\text{Nd}_{5.33}\text{EuTi}_{18}\text{O}_{54}$ ( $x=2/3$ )	78	10.46	10.4
$\text{Ba}_4\text{Nd}_{8.33}\text{DyTi}_{18}\text{O}_{54}$ ( $x=2/3$ )	78.6	10.04	33.8
$\text{Ba}_4\text{Sm}_{8.08}\text{Li}_{0.25}\text{Ti}_{18}\text{O}_{54}$ ( $x=2/3$ )	82.1	5.62	-2
$\text{Ba}_{4.2}(\text{Sm}_{0.9}\text{La}_{0.1})_{9.2}\text{Ti}_{18}\text{O}_{54}$ ( $x=0.6$ )	84	9.05	1.6
$\text{Ba}_{4.5}(\text{Nd}_{0.8}\text{Bi}_{0.2})_9\text{Ti}_{18}\text{O}_{54}$ ( $x=0.5$ )	106	4.2	8
$\text{Ba}_4(\text{La}_{1-y-z}\text{Sm}_y\text{Bi}_z)_{9.33}\text{Ti}_{18}\text{O}_{54}$ ( $x=2/3, y=0.7, z=0.04$ )	88.4	6.69	1
$\text{Ba}_4(\text{Sm}_{1-y}\text{Nd}_y)_{9.33}(\text{Ti}_{9.95}\text{Sn}_{0.05})\text{O}_{54}$ ( $x=2/3, y=0.8, z=0.05$ )	80	10.6	11
$\text{Ba}_4\text{Sr}_2\text{Nd}_8\text{Ti}_{18}\text{O}_{54}$ ( $x=0$ )	98.0	6	20
$(\text{Ba}_{1-\alpha}\text{Sr}_\alpha)_6\text{Sm}_8\text{Ti}_{18}\text{O}_{54}$ ( $x=0, \alpha=0.32$ )	91.3	8.02	61
$(\text{Ba}_{1-\alpha}\text{Sr}_\alpha)_{5.7}\text{Sm}_{8.2}\text{Ti}_{18}\text{O}_{54}$ ( $x=0.1, \alpha=0.298$ )	85.3	8.71	24
(h) (111) type layered perovskite ( $\text{Ba}_n\text{La}_4\text{Ti}_{3+n}\text{O}_{12+3n}$ -type homologous series)			

$\text{Ba}_x\text{La}_4\text{Ti}_{3+x}\text{O}_{12+3x}$ ( $x=0.2$ ) <sup>55)</sup>	42	86	-17
$\text{CaLa}_4\text{Ti}_4\text{O}_{15}$ ( $n=1$ )	41.1	50.2	-25
$\text{SrLa}_4\text{Ti}_4\text{O}_{15}$ ( $n=1$ )	43.8	50.2	-14
$\text{BaLa}_4\text{Ti}_4\text{O}_{15}$ ( $n=1$ )	45	47	-11
$\text{Ba}(\text{La}_{1-y}\text{Al}_y)_4\text{Ti}_4\text{O}_{15}$ ( $n=1, y=0.11$ )	44	47	1.3
$\text{Ca}(\text{La}_{0.875}\text{Nd}_{0.125})_4\text{Ti}_4\text{O}_{15}$ ( $n=1$ )	43.4	32.9	-13
$\text{Ba}_2\text{La}_3\text{Ti}_3\text{NbO}_{15}$ ( $n=1$ )	42.8	21.7	-8
$\text{Ba}_3\text{La}_2\text{Ti}_2\text{Nb}_2\text{O}_{15}$ ( $n=1$ )	49.4	20.2	4
$\text{Ba}_3\text{Nd}_2\text{Ti}_2\text{Nb}_2\text{O}_{15}$ ( $n=1$ )	46.8	19.5	28
$\text{Ba}_4\text{NdTiNb}_3\text{O}_{15}$ ( $n=1$ )	38.2	18.7	12
$\text{Ba}_2\text{La}_4\text{Ti}_5\text{O}_{18}$ ( $n=2$ )	46	31.85	-36
$\text{Ca}_2\text{La}_4\text{Ti}_5\text{O}_{18}$ ( $n=2$ )	44.7	20.1	6
(i) (100) type layered perovskite ( $A_{n+1}B_nO_{2n+1}$ Ruddlesden-Popper phase)			
$\text{Sr}_2\text{TiO}_4$ ( $n=1$ ) No.323[1]	15	1,600	-
$\text{Sr}_2\text{TiO}_4$ ( $n=1$ ) No.1273[1]	37.4	8,160	137
$\text{Sr}_3\text{Ti}_2\text{O}_7$ ( $n=2$ ) No.785[1]	26	2,400	-
$\text{Sr}_3\text{Ti}_2\text{O}_7$ ( $n=2$ ) No.1738[1]	57.9	18,850	317
$\text{Sr}_4\text{Ti}_3\text{O}_{10}$ ( $n=3$ ) No.1422[1]	42	960	-
$\text{Sr}_4\text{Ti}_3\text{O}_{10}$ ( $n=3$ ) No.1880[1]	76.1	12,700	576
(j) (110) type layered perovskite ( $A_nB_nO_{3n+2}$ type homologous series)			
$\text{La}_2\text{Ti}_2\text{O}_7$ ( $n=4$ )	47	8,500	-10
$\text{Nd}_2\text{Ti}_2\text{O}_7$ ( $n=4$ )	36.5	16,400	-118
$\text{CaLa}_4\text{Ti}_5\text{O}_{17}$ ( $n=5$ )	53.7	17,400	-26

**Table 2.** Microwave dielectric properties of perovskite and perovskite related compounds. No. in (i) list are cited from Sebastian's data base (Book) [1].

$R^{3+}B^{3+}O_3$  compounds containing rare-earth ions ( $R$ ) in the  $A$ -site of the perovskite structure are one of simplest perovskite-type compounds [29]. As the  $R$  ion is trivalent, the  $B$  ion in the  $B$ -site should also be trivalent. Almost all rare earth ions (that is Y to Er) can occupy the  $A$ -site. In some compounds, the  $A$ -site can be occupied by two or more  $R$  ions. Compounds including Sc, Yb and Lu ions have not been reported because of their small radius size. The  $B$ -site is occupied by a single ion such as Al, Ga and B, and by a pair of ions that are either divalent or tetravalent such as  $\text{Mg}^{2+}\text{Ti}^{4+}$  [30, 31]. These  $RBO_3$ -type compounds as shown in Table 2(a) are preferred for microwave dielectrics because of their small dielectric losses. The crystal structure changes from trigonal to orthorhombic depending on the tolerance factor, as shown

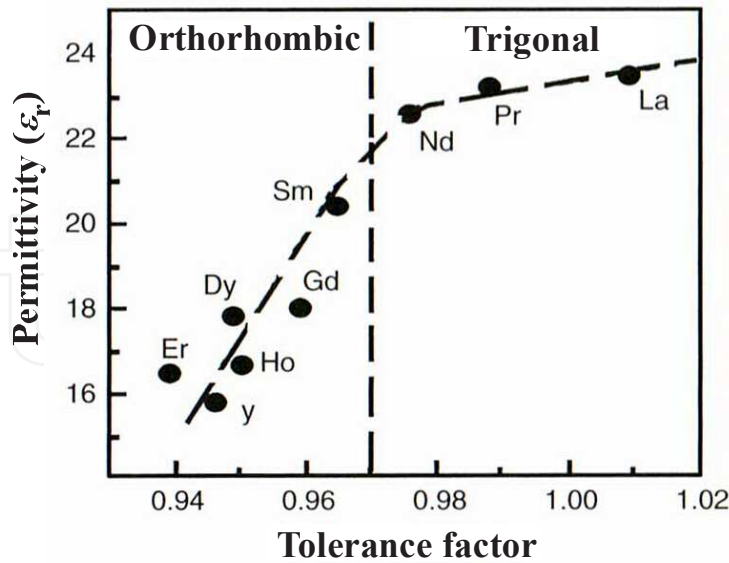


Figure 7. Variation of  $\epsilon_r$  as a function of the tolerance factor  $t$  in  $RAlO_3$ .

in Fig. 7 [29]. The compounds with a larger size of ion (La to Nd) are trigonal ( $R\bar{3}c$  No.167), and those with a smaller size (Sm to Er) are orthorhombic ( $Pnma$ , No.62).

The single crystals of  $LaAlO_3$  which can be grown easily from melts [32] are used as substrates for superconductor materials such as  $YBa_2Cu_3O_{7-x}$  because of their low dielectric losses and their small mismatch for epitaxial growth. It is noticed that strip-line resonators formed by superconductors grown epitaxially on the  $LaAlO_3$  single crystal substrate are used in the band-pass filter of base stations in microwave mobile communications. The low dielectric losses come from the low conductivity, based on zero electrical resistivity. Although the  $TCf$  of  $LaAlO_3$  is above  $-60$  ppm/°C [29], this is not an issue whenever it is used as the substrate for a superconductor at a fixed low temperature.

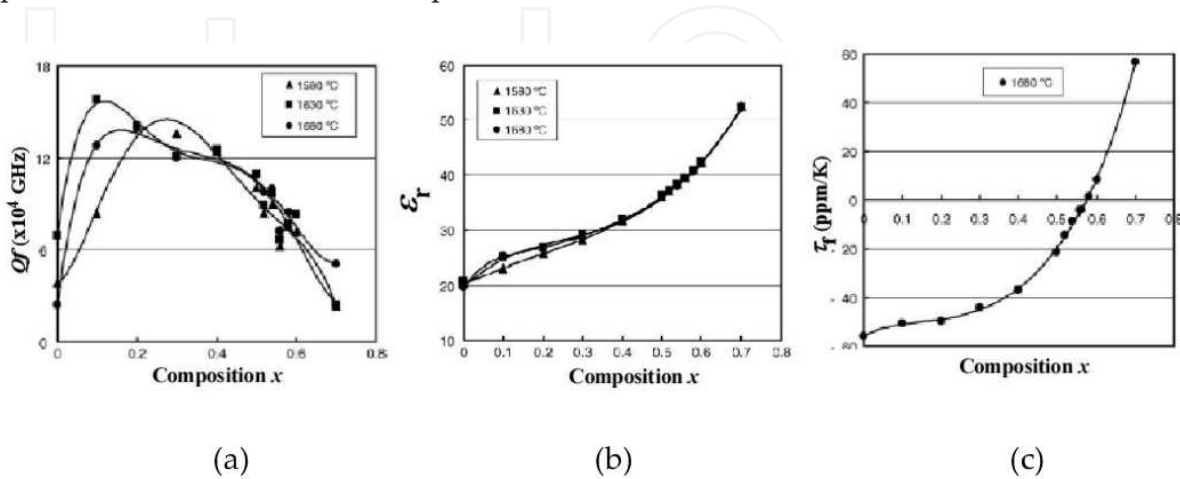
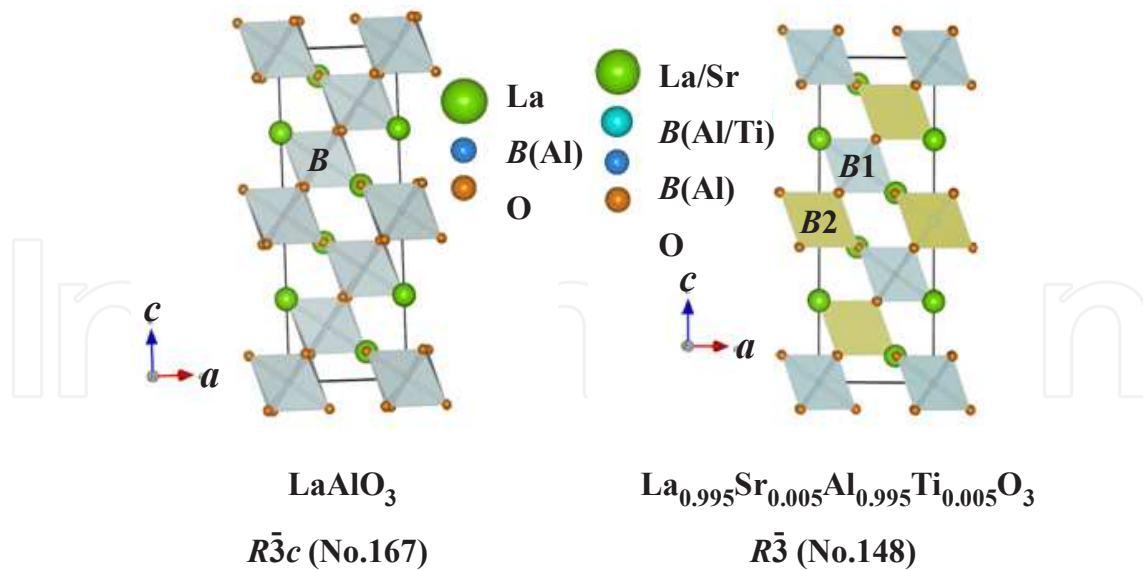


Figure 8.  $Q \cdot f$  value (a),  $\epsilon_r$  (b) and  $TCf$  (c) of  $(1-x)LaAlO_3-xSrTiO_3$  as a function of composition  $x$ .



**Figure 9.** Crystal structure of LaAlO<sub>3</sub> (a) with Space Group  $R\bar{3}c$  (167), and of SrTiO<sub>3</sub> doped LaAlO<sub>3</sub> (b) with S.G.  $R\bar{3}$  (148).

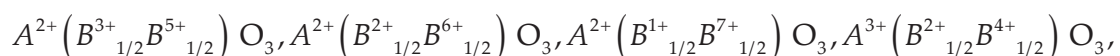
The  $TCf$  value is problematic whenever it is used as a resonator or filter at room temperature. In such cases, it is proposed that the  $TCf$  value is suppressed to near zero ppm/°C by the doping of SrTiO<sub>3</sub> or CaTiO<sub>3</sub> as shown in Fig. 8(c) [33, 34]. As these solid solutions show a high  $Q$  and a high  $\epsilon_r$  as shown in Fig. 8(a) and (b), the reason for the improved high  $Q$  value is seen through the study and analysis of a single crystal structure. Inagaki *et al.* [35] showed that the crystal system changed from  $R\bar{3}c$  (No. 167) to  $R\bar{3}$  (No. 148), thereby creating a new position for the Sr ion, as shown in Fig. 9(b) [35–36], and the observed disappearance of the polysynthetic twin. These facts suggest the improvement of  $Q \cdot f$ . Moreover, a NdTiO<sub>3</sub>-CaTiO<sub>3</sub> solid solution system is used for microwave dielectrics with a higher  $\epsilon_r$  instead of LaAlO<sub>3</sub>-SrTiO<sub>3</sub> solid solutions. The properties are as follows: 0.2SrTiO<sub>3</sub>-0.8LaAlO<sub>3</sub> [34]:  $\epsilon_r = 26.7$ ,  $Q \cdot f = 139,000$  GHz and  $TCf = -50$  ppm/°C ; 0.67CaTiO<sub>3</sub>-0.33NdAlO<sub>3</sub> [37]:  $\epsilon_r = 41.98$ ,  $Q \cdot f = 42,900$  GHz and  $TCf = 45$  ppm/°C.

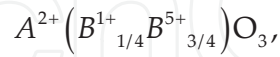
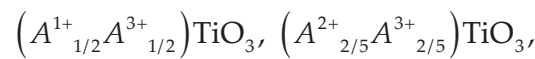
### 3.1.2. Complex perovskite

#### 3.1.2.1. Types of complex perovskite and their properties

Complex perovskite differs from simple perovskite by a single ion in both the A- and B-site. It is constituted maintaining the charge valance through the differently charged ions in each site, and is distinguished from the substance containing the substituted different plural ions. Complex perovskite compounds reported so far are as follows [38]:

#### 1:1 type in B-site



**1:2 type in B-site****1:3 type in B-site****1:1 type in A-site**

In the 1:2 type complex perovskite, many compounds exist with suitable properties. Tables 2(c), (d), (e) and (f) show characteristic microwave dielectrics with good properties selected from Sebastian's database, as referred to above [1, 2]. In the data, the microwave dielectric with the highest  $Q \cdot f$  value of 430,000 GHz is  $Ba(Mg_{1/3}Ta_{2/3})O_3$  (BMT) — the 'king' of microwave dielectrics [39]. The  $TCf$  also has a desirable value, being near to zero at 3.3 ppm/°C. The  $Q \cdot f$  value of  $Ca(Mg_{1/3}Ta_{2/3})O_3$  when Ca was substituted for Ba decreased to 78,000 GHz [40], and when Sr was substituted for Ba, it decreased even more, to 5,600 GHz [41]. Kageyama [42] showed the  $Q \cdot f$  values of 1:2 type complex perovskites as a function of the tolerance factor in the Ba and Sr-system as shown in Fig. 10. It brings a high  $Q \cdot f$  so that the tolerance factors of the Ba-system with large size ions in the A-site are large, and the electronic structure of the B-site ions is a closed shell. In the case of 1:1 type compounds,  $La(Mg_{1/2}Ti_{1/2})O_3$  (LMT) [43] shows the highest  $Q \cdot f$  of 114,000 GHz. The A-site of this compound is occupied by the trivalent rare earth La ion, and the valence of the B-site is trivalent and composed of the 1:1 ratio of  $Mg^{2+}$  and  $Ti^{4+}$ . However, the  $TCf$  of -81 ppm/°C is not a desirable value. Kageyama [44] systematically studied 1:1-type compounds and clarified that  $Ca(Ga_{1/2}Ta_{1/2})O_3$  (CGT) and  $Sr(Ga_{1/2}Ta_{1/2})O_3$  (SGT) show high a  $Q \cdot f$ . In this system, though the correlation with the tolerance factor is small, Ga with a closed shell electronic structure contributed to the improvement in  $Q \cdot f$  values. Wakino *et al.* [45] reported  $Ba(Mg_{1/2}W_{1/2})O_3$  (BMW) with a high  $Q \cdot f$ , composed of divalent Mg and six valenced W. These compounds also have the disadvantage of a large  $TCf$ . One of compounds with a near zero  $TCf$  is  $Ba(Tb_{1/2}Nb_{1/2})O_3$  (BTN) [46] with high  $\epsilon_r = 39$ ,  $Q \cdot f = 52,400$  GHz and  $TCf = -2$  ppm/°C.

**3.1.2.2. Is ordering a necessary condition for a high Q value?**

The origin of a high  $Q$  value, especially the relationship between a high  $Q$  value and ordering based on an order-disorder transition, has been under discussion for a long time [47, 51]. The feature of complex perovskite  $A(B_{1/3}B'_{2/3})O_3$  exhibits the phenomenon of the ordering of B cations. The ordered phase appeared at low temperature is low symmetry trigonal (rhombic-

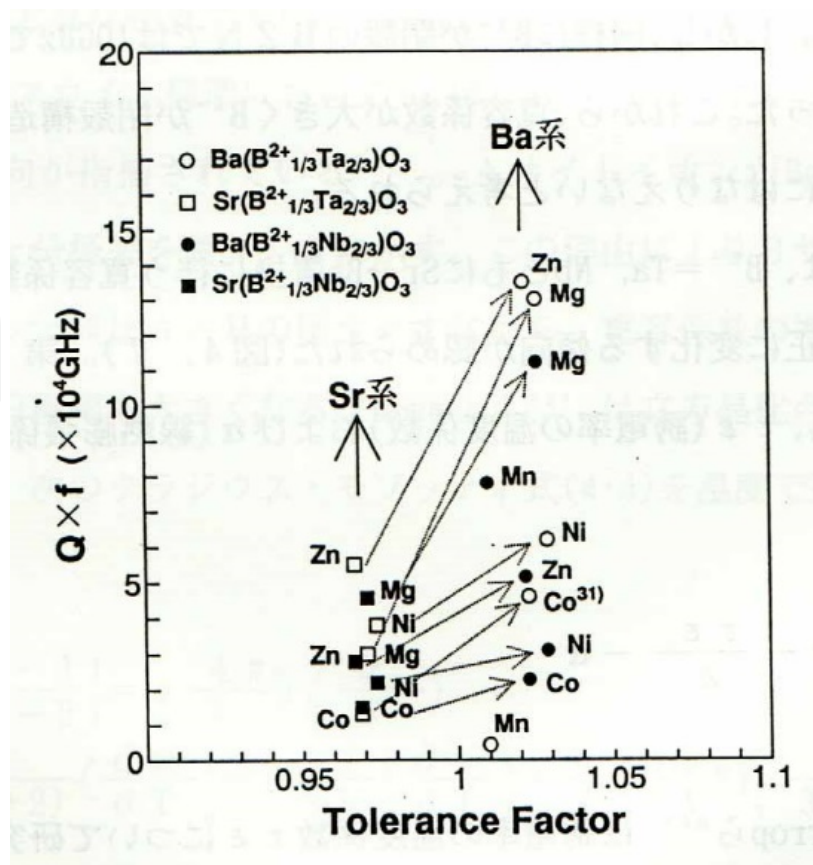


Figure 10.  $Q \cdot f$  of  $A(B^{2+}_{1/3}B^{5+}_{2/3})O_3$  as a function of the tolerance factor  $t$ .

hedral) structure of space group  $P\bar{3}m1$  (No. 164) and the disordered phase appeared at high temperature is high symmetry cubic structure of  $Pm\bar{3}m$  (No. 221) as shown in Fig. 11. Kawashima *et al.* [52] reported that  $Ba(Zn_{1/3}Ta_{2/3})O_3$  (BZT) has a high  $Q$ . BZT shows ordering of  $B$  cations, as revealed by the splitting and super structure lines on the X-ray powder diffraction (XRPD) patterns for a long sintering time. When the Zn and Ta ions occupy the same position, the structure is a disordered cubic one. On the other hand, if both ions occupy different independent sites, that is ordering, the structure becomes trigonal. This transition is sluggish and the temperature of transition is not clear in some compounds. The relationship between cubic and trigonal crystal structures is shown in Fig. 11. The  $B$  cations occupy the octahedra located between the hexagonal closed packing layers composing  $BaO_3$ . The ordering is apparent by the periodic arrangement of Zn-Ta-Ta along the  $c$ -axis of the trigonal. Though it is believed that ordering brings a high  $Q$ , some examples contradicting this have arisen, such as BMT- $Ba(Co_{1/3}Ta_{2/3})O_3$  [53] and  $Ba(Mg_{1/3}Ta_{2/3}Sn)O_3$  [54]. Recently, Koga *et al.* [55–59] presented the quantification of the ordering ratio using the Rietveld method and the ordering state in the vicinity of BZT. Kugimiya [60] reported that the composition which deviated from BMT has a high  $Q$  because of the high density composition. More recently Surendran *et al.* [61] showed that Ba and Mg deficient BMT compositions have a high  $Q$ . In this section, the author presents the primary factors for a high value of  $Q$  instead of ordering based on Koga's data [55–59, 61, 62].

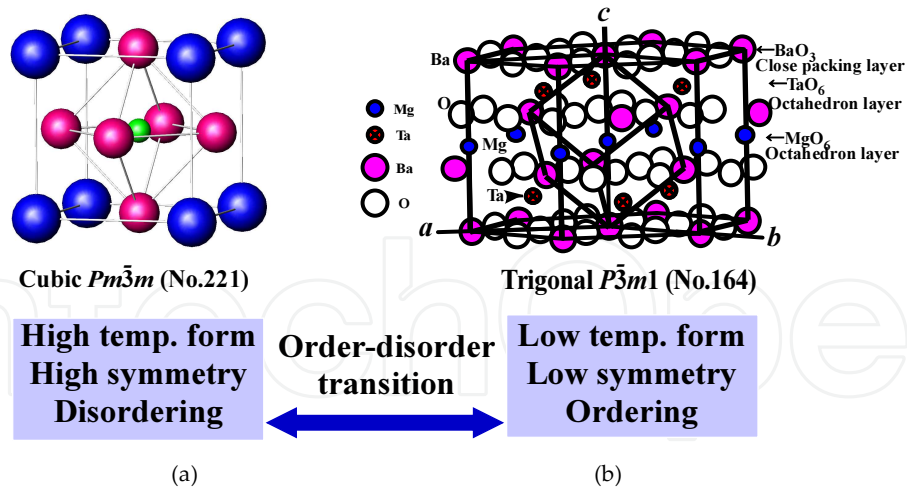


Figure 11. Order-disorder transition of perovskite. (a) High temperature and high symmetry phase with cubic, (b) Low temperature and low symmetry phase with trigonal.

• Ordering ratio and  $Q \cdot f$  [55]

Fig. 12 shows the XRPD patterns (a) and the high angle diffraction peaks (b) of BZT ceramics as a function of sintering time at 1,350 °C. According to sintering time, superlattice lines (asterisked) became clear and the 420 cubic diffraction peak splits gradually into two peaks, namely 226 and 422, in the trigonal system. It is considered that ordered and disordered structures coexist and ordered peaks become intense on sintering of 80 hours or more. These results are consistent with the report by Kawashima *et al* [52].

Fig. 13 shows  $Q \cdot f$  as functions of ordering ratio (a) obtained by the Rietveld method [63], density (b) and grain size (c). The ordering ratio saturates at about 80 % but the  $Q \cdot f$  varies from 40,000 to 100,000 GHz. However, the  $Q \cdot f$  increases with density and grain size. This indicates that the effect of ordering on the  $Q$  value is not so important.

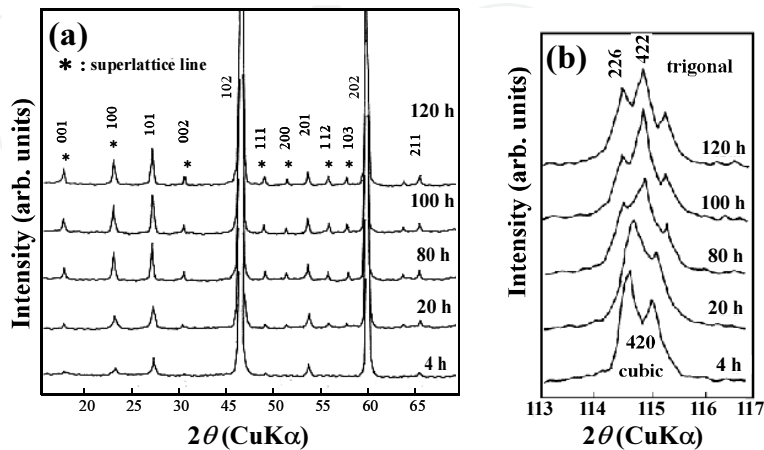


Figure 12. (a) XRPD patterns of BZT ceramics with different sintering time at 1,350 °C. Asterisks are superlattice reflections. (b) Magnified XRPD patterns around  $2\theta = 115^\circ$  in which 420 diffraction peak split to 226 and 422.

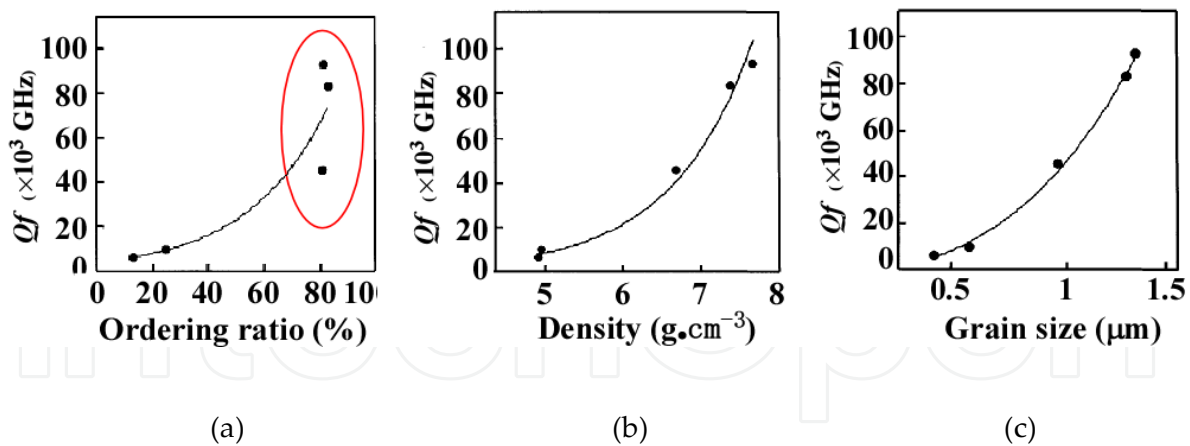
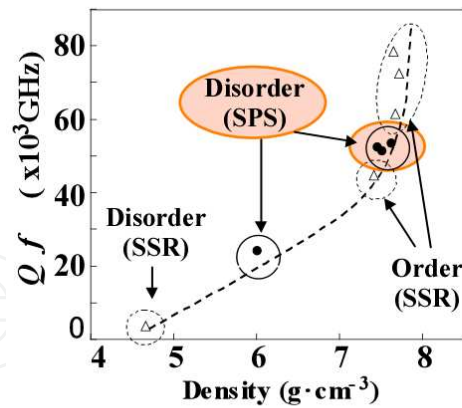


Figure 13. The  $Q \cdot f$  of BZT ceramics as functions of ordering ratio (a), density (b), and grain size (c).

- **Disordered BZT with a high  $Q \cdot f$  sintered by SPS [57]**

As both ordered and disordered BZT — with similar microstructures — can be obtained by various heat treatments using a conventional solid state reaction (SSR) as described in the previous section, the effects of the crystal-structural ordering and ceramic microstructure were discussed independently. In the case of BZT, although the high density and high  $Q$  ceramics of ordered BZT were synthesized by SSR with a long sintering time of over 80 hours, the dense ceramics of disordered BZT have not been obtained by SSR. Koga *et al.* [57] created high density disordered BZT ceramics with a short sintering time by spark plasma sintering (SPS). In this section, the effects of crystal-structural ordering and ceramic microstructure on the high  $Q$  are discussed.

Fig. 14 shows the  $Q \cdot f$  as a function of the densities in BZT fabricated using SSR and SPS. The samples obtained by SPS were of the disordered cubic type of perovskite as shown in the XRPD pattern (Fig. 15) with a lone 422 reflection compared with the ordered trigonal type with peak separations of 422 and 226 when sintered using SSR (1400 °C 100 h). The SPS samples with high densities were obtained using an extremely short sintering time of 5 mins between 1150 and 1300 °C under 30 Mpa [57]. The short time sintering when using SPS may result in the disordered BZT with a high density of 7.62  $\text{g}/\text{cm}^3$ , which is approximately 50% higher than that of low density samples of 5.0-6.0  $\text{g}/\text{cm}^3$  synthesized by conventional SSR. The full width at half maximum (FWHM) of the 420 peak became narrower with an increase in the temperature from 1,100 to 1,300 °C (Fig. 15). This indicates that the degree of crystallization of the disordered cubic phase is improved without the need for conversion to the ordered trigonal phase. Regardless of the method of synthesis,  $Q \cdot f$  is strongly dependent on density, and  $Q \cdot f$  values were improved with density as shown in Fig. 14. The highly crystallized dense disordered BZT ceramics synthesized by SPS showed a significantly high  $Q \cdot f$  (= 53,400 GHz) similar to that of the ordered BZT sample with the same density (= ca. 7.5  $\text{g}/\text{cm}^3$ ) synthesized by SSR. The crystallization with densification of BZT ceramics should play a more important role in the improvement of the  $Q$  factor in the BZT system than structural ordering and grain size. In the high density region ( $> 7.5 \text{ g}/\text{cm}^3$ ), the variation of the  $Q \cdot f$  should be clarified.



**Figure 14.**  $Q \cdot f$  of BZT by solid state reaction (SSR) and spark plasma sintering (SPS) as a function of density. Order: ordered perovskite, Disorder: disordered perovskite.

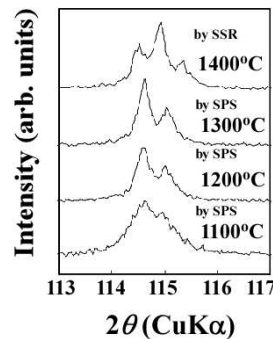


**Figure 15.** XRPD patterns around 420 diffraction of BZT sintering by SPS for 5 min under 30 MPa with different sintering temperature.

- **Ba(Zn<sub>1/3</sub>Nb<sub>2/3</sub>)O<sub>3</sub> (BZN) with clear order-disorder transition [58]**

Ordering based on the order-disorder transition brings low symmetry, and disordering brings high symmetry as described above. Usually, high symmetry also brings a high  $Q$ , similar to ordering. We present an example showing that high symmetry is more influential in bringing about a high  $Q$  than ordering is.

BZN clearly shows an order-disorder transition temperature at 1,350 °C as shown in Fig. 16 (a). The transition temperatures of BMT and BZT are unclear because of the high transition temperature. The ordering was confirmed using X-ray diffraction patterns. Fig. 16 shows  $Q \cdot f$ , grain size and density as a function of the sintering temperature of BZN. The disordered sample sintered at 1,400 °C shows a drastic increase of  $Q \cdot f$ , grain size and density when compared with ordered samples sintered at 1,200 and 1,300 °C. As a result of the post-annealing at 1,200 °C over 100h for the disordered sample sintered at 1,400 °C, the structure transformed to order, but the  $Q \cdot f$  did not improve and instead it decreased slightly in an inverse manner. The grain sizes and densities were not changed by the annealing, as shown in Figs. 16(b) and (c).

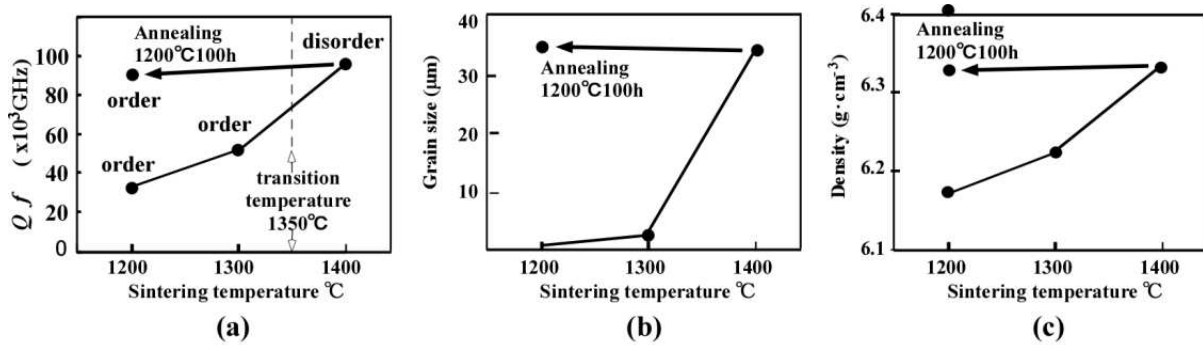


Figure 16.  $Q \cdot f$  (a), grain size (b) and density (c) of BZN with transition temperature at 1350 °C as a function of sintering temperature. Although the disorder phase with a high  $Q$  sintered at 1400 °C annealed at 1200 °C, the  $Q \cdot f$  did not improve.

Therefore, we can conclude that the crystal-structural ordering in the ceramic BZN system has no significant effect on the improvement of the  $Q$  factor. The  $Q$  factor strongly depends on the density and grain size, but not on the crystal-structure order. The decrease in  $Q \cdot f$  as a result of annealing might be dependent on the low symmetry that accompanies ordering.

### 3.1.2.3. Phase relations and $Q \cdot f$ in the vicinity of BZT [56, 59]

- Koga’s research on BZT

Koga *et al.* [56, 59] studied the phase relation in the vicinity of BZT in the BaO-ZnO-TaO<sub>5/2</sub> ternary system as shown in Fig. 17. These samples were sintered at 1,400 °C for 100 hours as reported in Koga’s paper [56]. These diffraction patterns fit the Rietveld method well [63]. Ordering ratios obtained are shown in Fig. 18(a). Three areas in the vicinity of BZT are presented as shown in Fig. 17.

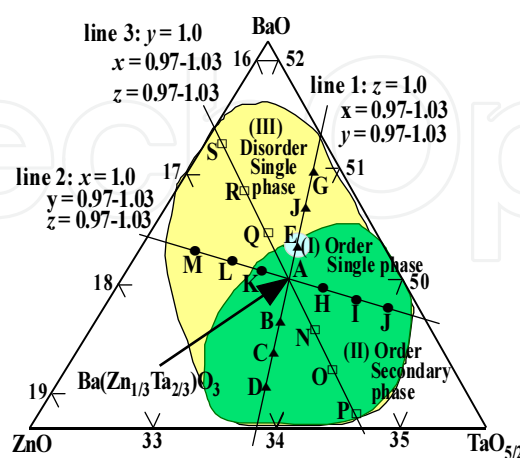


Figure 17. BaO-ZnO-TaO<sub>5/2</sub> partial ternary system in the vicinity of BZT. Synthesized compositions are shown by the letters A to S. The A point is pure BZT. Three areas are shown and these are (I) for order/single phase, (II) for order/secondary phase, and (III) for disorder/single phase.

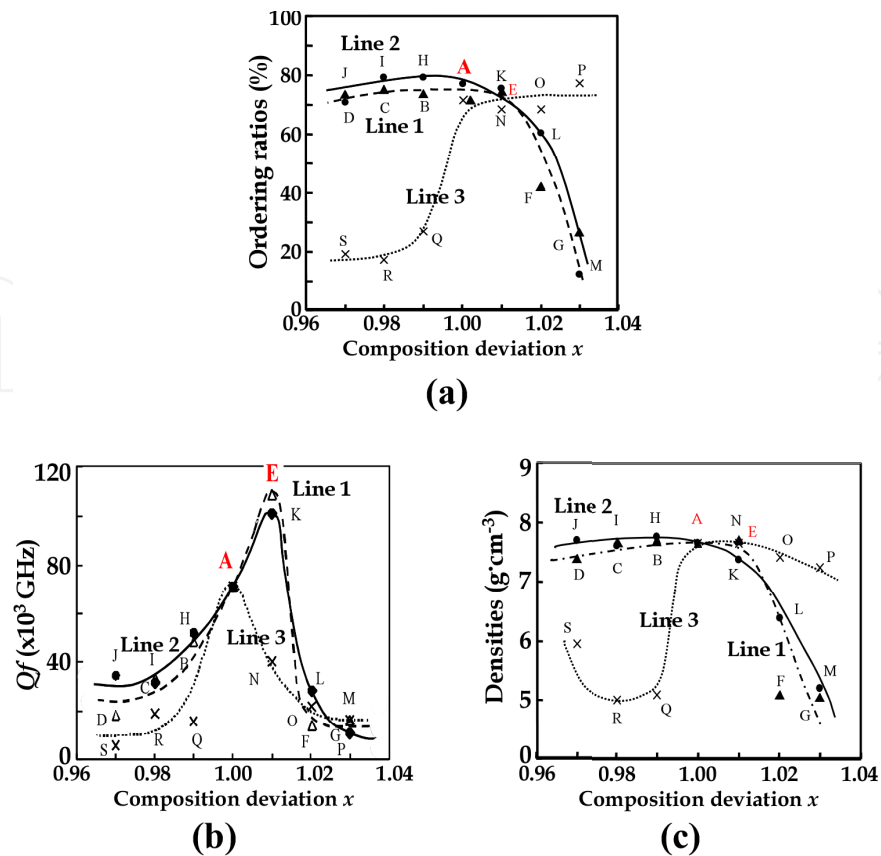


Figure 18. Ordering ratio (a),  $Q \cdot f$  (b) and density (c) as a function of composition deviation from pure BZT.

(I): Ordering area with BZT single phase

(II): Ordering area with secondary phase

(III): Disordering area with BZT single phase

The first area (I) is composed of a single phase of BZT with an ordered structure and a high  $Q \cdot f$ . The compositions E and K have a  $Q \cdot f$  about 50 % higher than that of the pure BZT composition A. Composition K is located on the boundary area (I) and has a minor secondary phase as revealed by the SEM figure reported in a previous paper [59]. The ordering ratio in composition E is lower than A, and the density of composition E is same as that of A. The second area (II) is an ordered BZT with a secondary phase  $\text{BaTa}_2\text{O}_6$  with a specific amount of Zn [59] analyzed by X-ray microanalyzer (XMA). The ordering ratio of compounds located in this area is high at about 70 to 80 % as shown in Fig. 18(a). Although the structure is ordered, the  $Q \cdot f$  values decrease according to the deviation from pure BZT as shown in Fig. 18(b). The composition of the ordered BZT compounds is located on  $\text{Ta}_2\text{O}_5$  rich side, which is precipitated with secondary phase as a eutectic phase diagram system. The third area (III) is precipitated as a single phase BZT solid solution with a disordered structure. The  $Q \cdot f$  values degrade with a decrease in the ordering ratio and density as shown in Fig. 18(c). The lower density comes from the existence of numerous pores due to hard sintering. The single phase in this area is originated by a solid solution accompanying defects in B- and O-sites, which causes degrada-

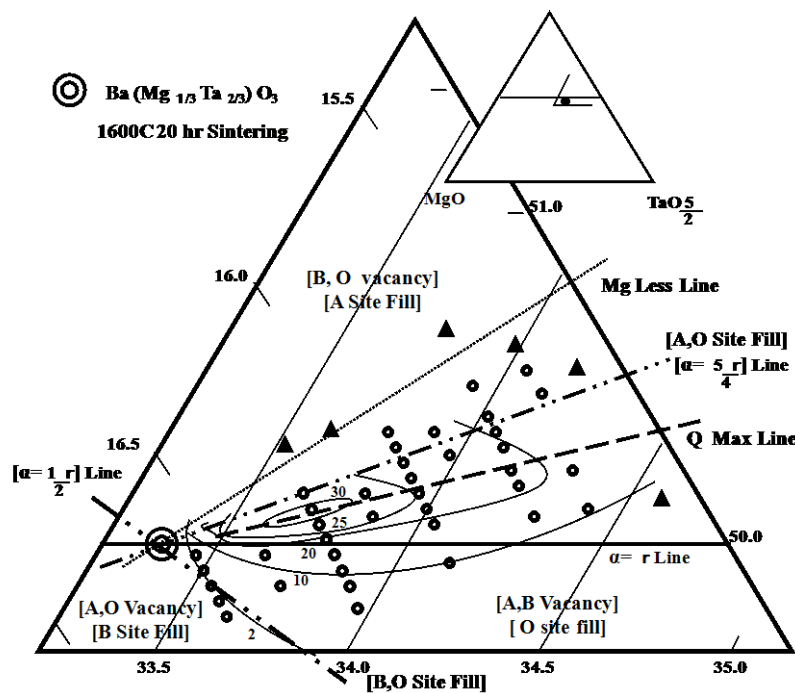


**Figure 19.** Partial BaO-MgO-TaO<sub>5/2</sub> ternary system in the vicinity of BMT. On the tie line BMT-BaTa<sub>4/5</sub>O<sub>3</sub>, Ba(Mg<sub>1/3-α/3</sub>Ta<sub>2/3+2α/15</sub>V<sub>α/5</sub>)O<sub>3</sub> solid solutions are formed with high densities and high Q values, in which A- and O-sites are filled, and the B-site has vacancies without charge. Three areas are divided by two lines:  $\alpha = 5\gamma/4$  and  $\alpha = \gamma/2$ . The first one is B- and the O-site is vacant although the A-site is filled. The second one is A- and the B-site is vacant although the O-site is filled. The third one is A- and the O-site has vacancies, although the B-site is filled.

tion of  $Q \cdot f$ . The pores and defects were examined by SEM [59] and Raman scattering spectra [62] respectively.

• **Kugimiya's research on BMT/BMT** [60, 61]

Kugimiya [60] presented the highest  $Q \cdot f$  composition at the Ta and Ba rich side in a BMT system as shown in Fig. 19. The synthesized samples are precise compositions formed by master batches which mixed samples from the four master batch method. Here, chemical formulae in the vicinity of BMT are reported as follows: Kugimiya presented three areas divided by drawing two lines as shown in Table 3 and Fig. 19.

$\alpha$	Chemical formula	Vacancy
$\alpha > 5\gamma/4$	$Ba_{1+\alpha}(Mg_{1/3}Ta_{2/3+\gamma}V_{\alpha-\gamma})O_{3+\alpha+5\gamma/2}V_{2\alpha-5\gamma/2}$	A: fill, B, O: vacancy
$\alpha = 5\gamma/4$	$Ba_{1+\alpha}(Mg_{1/3}Ta_{2/3+4\alpha/5}V_{\alpha/5})O_{3+3\alpha}$	A, O: fill, B: vacancy
$5\gamma/4 > \alpha > \gamma/2$	$Ba_{1+\alpha}V_{5\gamma/6-2\alpha/3}(Mg_{1/3}Ta_{2/3+\gamma}V_{\alpha(3-\gamma/6)})O_{3+\alpha+5\gamma/2}$	A, B: vacancy, O: fill
$\alpha = \gamma/2$	$Ba_{1+\alpha}V_{\alpha}(Mg_{1/3}Ta_{2/3+\gamma})O_{3+6\alpha}$	A: vacancy, B, O: fill
$\alpha < \gamma/2$	$Ba_{1+\alpha}V_{\gamma-\alpha}(Mg_{1/3}Ta_{2/3+\gamma})O_{3+\alpha+5\gamma/2}V_{\gamma/2-\alpha}$	A, O: vacancy, B: fill

**Table 3.** Chemical formula for three areas divided by two lines:  $\alpha = 5\gamma/4$  and  $\alpha = \gamma/2$ , here,  $\alpha$  and  $\gamma$  are in Ba<sub>α</sub>Ta<sub>γ</sub>O<sub>α+5γ/2</sub> and vacancies are on the A-, B- and O-sites.

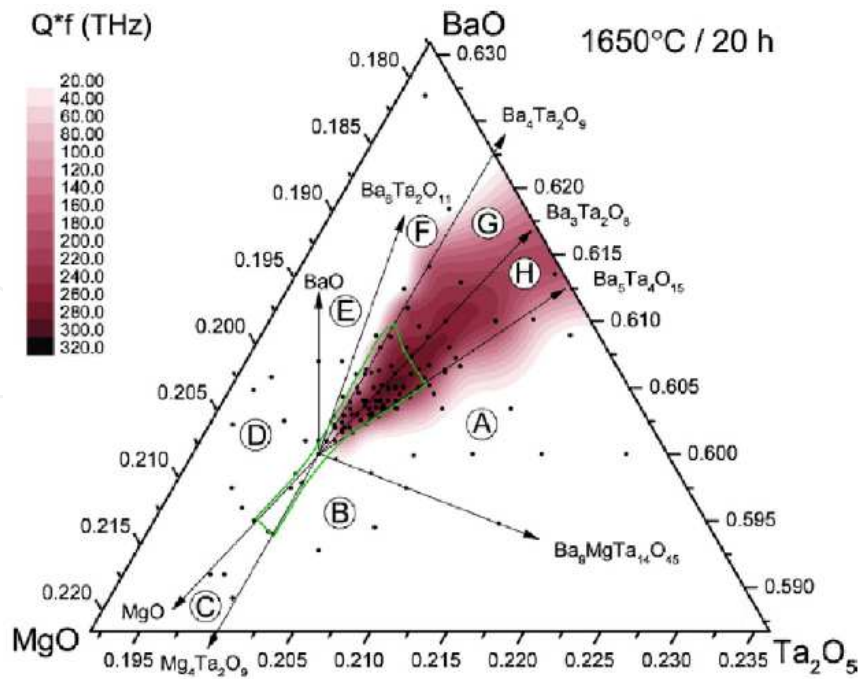


**Figure 20.** Part of the BaO–MgO–Ta<sub>2</sub>O<sub>5</sub> phase diagram in the vicinity of the BMT phase indicating a composition dependence of the  $Q \cdot f$  for samples sintered at 1650 °C for 20 h. Small black dots indicate the target sample compositions. Green line indicates an approximate boundary of the single-phase BMT.

Here,  $\alpha$  and  $\gamma$  are in  $\text{Ba}_\alpha\text{Ta}_\gamma\text{O}_{\alpha+5\gamma/2}$ . In the region  $\alpha > 5\gamma/4$ , the composition denoted by  $\text{Ba}_{1+\alpha}(\text{Mg}_{1/3}\text{Ta}_{2/3+\gamma}\text{V}_{\alpha-\gamma})\text{O}_{3+\alpha+5\gamma/2}\text{V}_{2\alpha-5\gamma/2}$  has B- and O-site vacancies with holes and electrons. In the  $\alpha = 5\gamma/4$  line, the compositions denoted by  $\text{Ba}_{1+\alpha}(\text{Mg}_{1/3}\text{Ta}_{2/3+4\alpha/5}\text{V}_{\alpha/5})\text{O}_{3+3\alpha}$  are the ideal ones without vacancies in the A- and O- sites. The B-site vacancy is neutralized without charge. The highest  $Q \cdot f$  composition is located near the line  $\alpha = 5\gamma/4$  as shown in Fig. 19. The compositions in the line are ideal for microwave dielectrics because there are no oxygen defects and the density is high due to the substitution of Ta for Mg. In the region  $5\gamma/4 > \alpha > \gamma/2$ , the composition denoted by  $\text{Ba}_{1+\alpha}\text{V}_{5\gamma/6-2\alpha/3}(\text{Mg}_{1/3}\text{Ta}_{2/3+\gamma}\text{V}_{\alpha/3-\gamma/6})\text{O}_{3+\alpha+5\gamma/2}$  has a defect in the A- and B-sites filled with holes and electrons. In the region at  $\alpha = \gamma$ , the composition denoted by  $\text{Ba}_{1+\alpha}\text{V}_{\alpha/6}(\text{Mg}_{1/3}\text{Ta}_{2/3+\alpha}\text{V}_{\alpha/6})\text{O}_{3+7\alpha/2}$  has the same amount of vacancies in both A- and B-sites filled with the same holes and electrons. In the region  $\alpha = \gamma/2$ , the composition denoted by  $\text{Ba}_{1+\alpha}\text{V}_\alpha(\text{Mg}_{1/3}\text{Ta}_{2/3+\gamma})\text{O}_{3+6\alpha}$  only has vacancies in the A-site with holes and in the B-site with excess electrons which introduced instability. In the region  $\alpha < \gamma/2$ , the composition denoted by  $\text{Ba}_{1+\alpha}\text{V}_{\gamma-\alpha}(\text{Mg}_{1/3}\text{Ta}_{2/3+\gamma})\text{O}_{3+\alpha+5\gamma/2}\text{V}_{\gamma/2-\alpha}$  has holes in both the A- and O-sites with electrons and excess electrons in the B-site, which leads to an unstable crystal structure.

The contour lines in Fig. 19 show  $Q$  values from 2,000 in the outer area to 30,000 in the center. The highest  $Q$  value of 50,000 was obtained in the center. The contour is elongated parallel to the  $Q$  max line as drawn in Fig. 19 and it changes steeply on the perpendicular to the line.

- **Kolodiazhnyi's research on BMT [64]**

The author presented a part of the BaO–MgO–Ta<sub>2</sub>O<sub>5</sub> phase diagram in the vicinity of the BMT phase as shown in Fig. 20 [64]. Ceramic samples whose chemical composition falls within the

A, B and C compositional triangles (CTs) in Fig. 20 reach a relative density of 96–98% after sintering at 1,550–1,580 °C for 20 hours. Samples located in the H and G CTs required temperatures of 1,630–1,650 °C to reach a relative density of 96–98 %. The specimens located in the D, E and F CTs retained a density of  $\leq 80\%$  after heat treatment at 1,680 °C. The pure BMT sintered at 1,650 °C for 20 h shows a poor dielectric performance with a  $Q \cdot f \approx 20,000\text{--}40,000$  GHz. A very large variation in the dielectric properties and density of ceramics was found upon a slight deviation from pure BMT composition. The tendency of the variation was similar to Koga's results as shown in Fig. 17 [56]. Significant improvement in the  $Q \cdot f$  values is seen in samples with a slight Mg deficiency, which are located in the G and H CTs. The highest  $Q \cdot f$  compositions of 330,000–340,000 GHz were found within the H CT close to the BMT-Ba<sub>3</sub>Ta<sub>2</sub>O<sub>8</sub> tie line. Upon approaching the BMT-Ba<sub>5</sub>Ta<sub>4</sub>O<sub>15</sub> tie line from the H CT, the  $Q \cdot f$  starts to decrease and then drops sharply after crossing into the A CT. Mg-rich BMT with a high density and a high degree of 1:2 cation order within B and C CTs showed low  $Q \cdot f$  values (e.g.  $Q \cdot f < 20,000$  GHz). The dominant source of the extrinsic dielectric loss is identified as Mg occupation substituted for Ba in the A-site (Mg<sub>Ba</sub>) which improves 'rattling' inside the dodecahedral position. Ta-poor, non-pure BMT samples located in the D, E and F CTs showed a very low density and high dielectric losses after sintering at 1,650 °C for 20 h.

- **High Q by high density composition** [60, 61]

Koga's data [56] and Kolodiazhnyi's [64] data are comparable with Kugimiya's BMT data [60]. The area (I) and the H CT with the highest  $Q \cdot f$  as shown in Figs 17 and 20 respectively, are located on the opposite side of Kugimiya's data against the BMT-Ba<sub>5</sub>Ta<sub>4</sub>O<sub>15</sub> tie line (Fig. 19). These compositions will be comparable with the completed ideal crystal structure Ba<sub>1+α</sub>(Mg<sub>1/3</sub>Ta<sub>2/3+4α/5</sub>V<sub>α/5</sub>)O<sub>3+3α</sub> reported by Kugimiya [60]. The formula is rewritten as Ba(Mg<sub>1/3-α/3</sub>Ta<sub>2/3+2α/15</sub>V<sub>α/5</sub>)O<sub>3</sub> solid solutions on the tie-line BMT-Ba<sub>5</sub>Ta<sub>4</sub>O<sub>15</sub>. The crystal structure in the composition region is perfect, without defects, and with a high density. The density of BMT increases with the introduction of the Ba<sub>5</sub>Ta<sub>4</sub>O<sub>15</sub> phase, because Mg ions are substituted by heavy Ta ions.

Surendran *et al.* [61] also presented compositions with high Q values in the two kinds of magnesium and barium deficient nonstoichiometric compositions Ba(Mg<sub>1/3-x</sub>Ta<sub>2/3</sub>)O<sub>3</sub> [ $x=0.015$ ] and Ba<sub>1-x</sub>(Mg<sub>1/3</sub>Ta<sub>2/3</sub>)O<sub>3</sub> [ $x=0.0075$ ] as shown in Fig. 21(a). The microwave dielectric properties of Ba<sub>0.9925</sub>(Mg<sub>0.33</sub>Ta<sub>0.67</sub>)O<sub>3</sub> [ $\epsilon_r = 24.7$ ,  $TCf = 1.2$  ppm/°C,  $Q \cdot f = 152,580$  GHz] and Ba(Mg<sub>0.3183</sub>Ta<sub>0.67</sub>)O<sub>3</sub> [ $\epsilon_r = 25.1$ ,  $TCf = 3.3$  ppm/°C and  $Q \cdot f = 120,500$  GHz] were found to be better than stoichiometric BMT [ $\epsilon_r = 24.2$ ,  $TCf = 8$  ppm/°C and  $Q \cdot f = 100,500$  GHz]. The important difference from Kugimiya's results [60] is standing on the nonstoichiometry with a barium or magnesium deficiency. We consider that Surendran's data [61] is based on Kugimiya's results [60]. In the case of Mg-deficient BMT, as the composition is located near Kugimiya's area with a high  $Q \cdot f$ , the composition of the main compound must be Ba(Mg<sub>1/3-α/3</sub>Ta<sub>2/3+2α/15</sub>V<sub>α/5</sub>)O<sub>3</sub> solid solutions on the tie-line BMT-Ba<sub>5</sub>Ta<sub>4</sub>O<sub>15</sub>. As shown in Fig. 21(b), in the solid solution area, the Mg deficiencies are filled with Ta and create vacancies in the B-site, so that density and the ordering ratio are maintained. On the other hand, the existing area of Ba-deficient BMT is included in Koga's (II) area as shown in Fig. 17, composed of ordered BMT and secondary phase. The ordered BMT will have a similar composition with a high

density and a high  $Q \cdot f$  on the BMT-Ba<sub>5</sub>Ta<sub>4</sub>O<sub>3</sub> tie-line presented by Kugimiya [60]. The compound by Surendran *et al.* [61] may be located in the eutectic phase diagram region accompanying the secondary phase. However, as the amount of secondary phases is small, detection may be difficult. Though the density and ordering ratio are maintained at a high level as shown in Fig. 21(c),  $Q \cdot f$  values degrade steeply according to the secondary phase. The compound should be stoichiometric and complete, because microwave dielectrics with a high  $Q$  are usually free of defects.

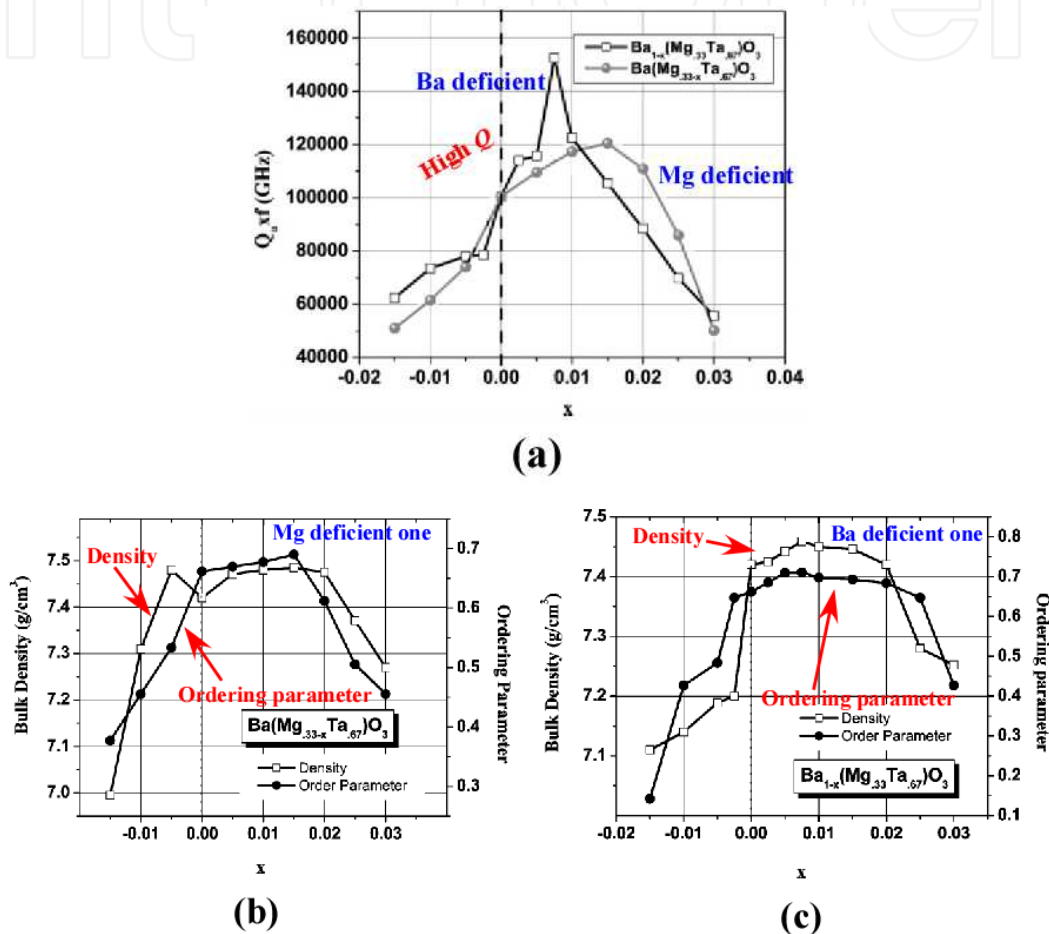


**Figure 21.** (a)  $Q \cdot f$  for  $\text{Ba}(\text{Mg}_{1/3-x}\text{Ta}_{2/3})\text{O}_3$  and  $\text{Ba}_{1-x}(\text{Mg}_{1/3}\text{Ta}_{2/3})\text{O}_3$  as a function of composition deviation ( $x$ ), (b) Bulk density and ordering parameter for  $\text{Ba}(\text{Mg}_{1/3-x}\text{Ta}_{2/3})\text{O}_3$  as a function of  $x$ , (c) Bulk density and ordering parameter for  $\text{Ba}_{1-x}(\text{Mg}_{1/3}\text{Ta}_{2/3})\text{O}_3$  as a function of  $x$ .

#### 3.1.2.4. Important points concerning complex perovskite

- A complex perovskite is composed of different ions with different charges such as  $A^{2+}$  ( $B^{2+}_{1/3}B^{5+}_{2/3}$ ) $\text{O}_3$ , thereby maintaining the charge valance.
- A complex perovskite usually has an order-disorder phase transition. The order phase is a low temperature phase with low crystallographic symmetry, while the disorder phase is a high temperature phase with high symmetry. In the case of a 1:3 type complex perovskite,

the ordered phase is a trigonal (rhombohedral)  $R\bar{3}c$  (No. 167), and the disorder phase is a cubic  $Pm\bar{3}m$  (No. 221) [55, 65].

- The  $Q \cdot f$  is dependent on the density instead of on ordering based on SPS sintering [57].
- In the case of a compound with an order-disorder phase transition, the disorder phase with high symmetry might show a high  $Q \cdot f$  instead of the order phase, based on the results of BZN [58, 65].
- In the vicinity of BZT in the BaO-ZnO-Ta<sub>2</sub>O<sub>5</sub> system, there are three areas, namely (I) an ordering area with a single phase; (II) an ordering area with a secondary phase and (III) a disordering area with a single phase [56, 66].
- The composition with the highest  $Q \cdot f$  should ideally be located on the tie-line BZT/BMT-BaTa<sub>4/5</sub>O<sub>3</sub>, on which Ba(Mg<sub>1/3-α/3</sub>Ta<sub>2/3+2α/15</sub>V<sub>α/5</sub>)O<sub>3</sub> solid solutions are formed. The composition shows a higher density than that of pure BZT/BMT [56,60, 67].

### 3.2. Perovskite related compounds

#### 3.2.1. Pseudo-tungsten-bronze solid solutions

##### • Crystal structure of pseudo-tungsten-bronze solid solutions

The pseudo-tungsten-bronze Ba<sub>6-3x</sub>R<sub>8+2x</sub>Ti<sub>18</sub>O<sub>54</sub> ( $R$  = rare earth) solid solutions [68, 69] are located on the perovskite-type compound tie-line of BaTiO<sub>3</sub> and R<sub>2</sub>Ti<sub>3</sub>O<sub>9</sub> compositions on the BaO-R<sub>2</sub>O<sub>3</sub>-TiO<sub>2</sub> ternary phase diagram as shown in Fig. 22. The crystal structure contains perovskite blocks of 2 x 2 unit cells (2x2), and pentagonal ( $A_2$ ) sites as shown in Fig. 23, which are named from similar tetragonal tungsten-bronze structure with 1x1 perovskite blocks [70–72]. These compounds contain two ions with different atomic sizes. The larger Ba ions are found mainly in the pentagonal  $A_2$ -site and the smaller rare-earth ( $R$ ) ions in the rhombic  $A_1$ -site. This structure has two more sites,  $B$  and  $C$ . The  $B$ -site is same as perovskite octahedral sites, and the  $C$ -site is a triangular site which is usually empty. This structure has a close relationship to the structure of perovskite. If the two ions become the same size, the structure changes to perovskite with only cubic  $A_1$ -sites owing to the combination of the  $A_2$  and  $C$ -sites as described later at section 4 (Fig. 40). The crystal data are as follows: orthorhombic crystal system of space group  $Pbnm$  (No.62), point group  $mmm$ , lattice parameter  $a = 12.13$ ,  $b = 22.27$ ,  $c = 7.64$  Å,  $Z = 2$ ,  $D_x = 5.91$  g/cm<sup>3</sup>. This structure has a super lattice along the  $c$ -axis of twice [73]. As the space group has a center of symmetry of  $i$  as do paraelectrics, it qualifies for microwave dielectrics. The chemical formula of all occupied sites is Ba<sub>6</sub>R<sub>8</sub>C<sub>4</sub>Ti<sub>18</sub>O<sub>54</sub> and the structural formula is  $[R_8Ba_2]_{A1}[Ba_4]_{A2}[V]_C[Ti_{18}]_B O_{54}$ , where  $V$  is vacancy. As this chemical formula is  $x = 0$ , the chemical formula of the solid solutions is Ba<sub>6-3x</sub>R<sub>8+2x</sub>Ti<sub>18</sub>O<sub>54</sub> and the structural formula is  $[Ba_4]_{A2}[Ba_{2-3x}R_{8+2x}]_{A1}Ti_{18}O_{54}$ . Here, the amount of Ba in the  $A_1$ -site becomes zero if  $2-3x = 0$ , that is,  $x = 2/3$ . This composition is special due to one factor : the structure formula is  $[Ba_4]_{A2}[R_{8+4/3}]_{A1}Ti_{18}O_{54}$  and is occupied separately by Ba in  $A_2$  and by  $R$  in  $A_1$  as shown in Fig. 24. This special composition is called “compositional ordering”.

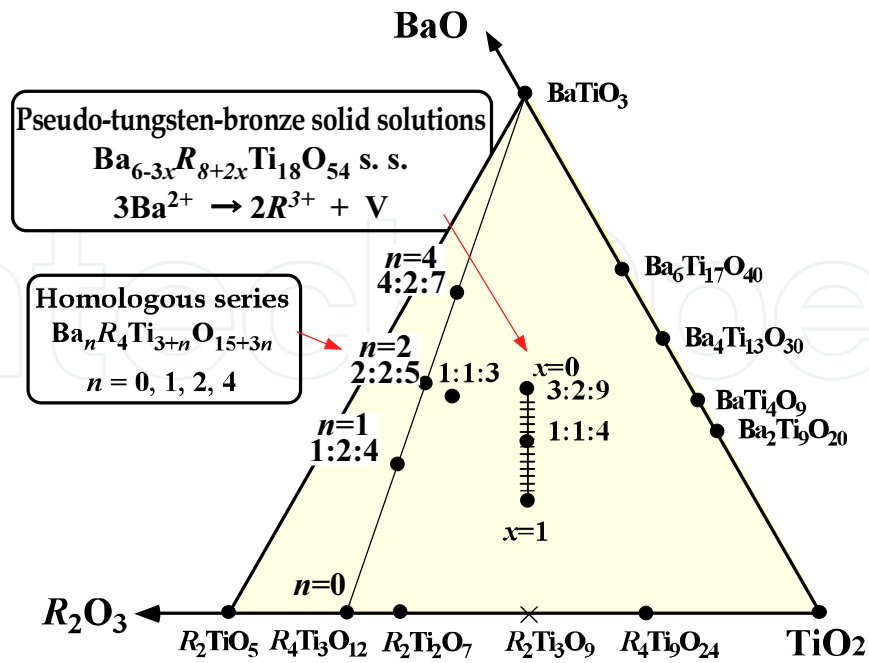


Figure 22. Part of the BaO-R<sub>2</sub>O<sub>3</sub>-TiO<sub>2</sub> ternary phase diagram with pseudo-tungsten-bronze type solid solutions and homologous compounds.

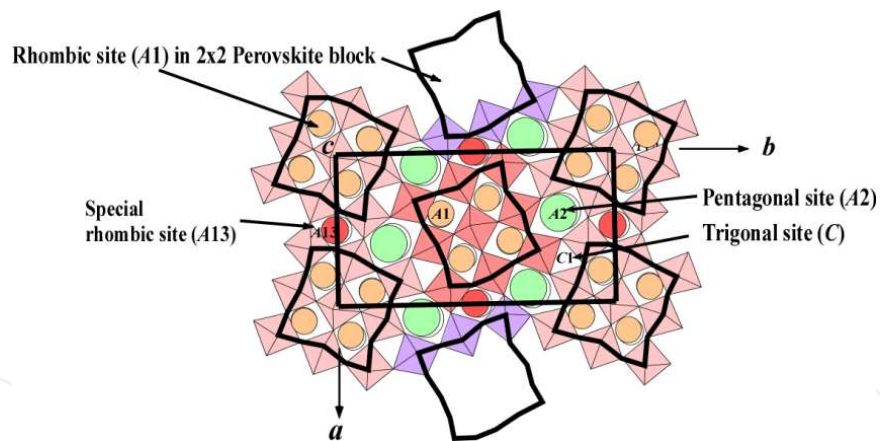


Figure 23. Crystal structure of the pseudo-tungsten-bronze solid solutions viewed in projection along [001]. Pentagonal sites (A<sub>2</sub>) are located among 2x2 perovskite blocks with rhombic sites (A<sub>1</sub>).

• Microwave dielectric properties of pseudo-tungsten-bronze solid solutions

The quality factor  $Q \cdot f$  of the  $x = 2/3$  composition, in which R and Ba ions separately occupy the rhombic site A<sub>1</sub> and the pentagonal site A<sub>2</sub> respectively, show the highest  $Q f$  values: 10,549 GHz in the Sm system, 10,010 GHz in the Nd system, and 2,024 GHz in the La system<sup>4)</sup> as shown in Fig.25 (a) [74]. The highest quality factor is based on the compositional ordering of R and Ba ions in the A<sub>1</sub> and A<sub>2</sub> sites respectively, as shown in Fig. 24. The ordering distribution of the ions reduces the internal strain and results in the non-linear variation in quality factor.

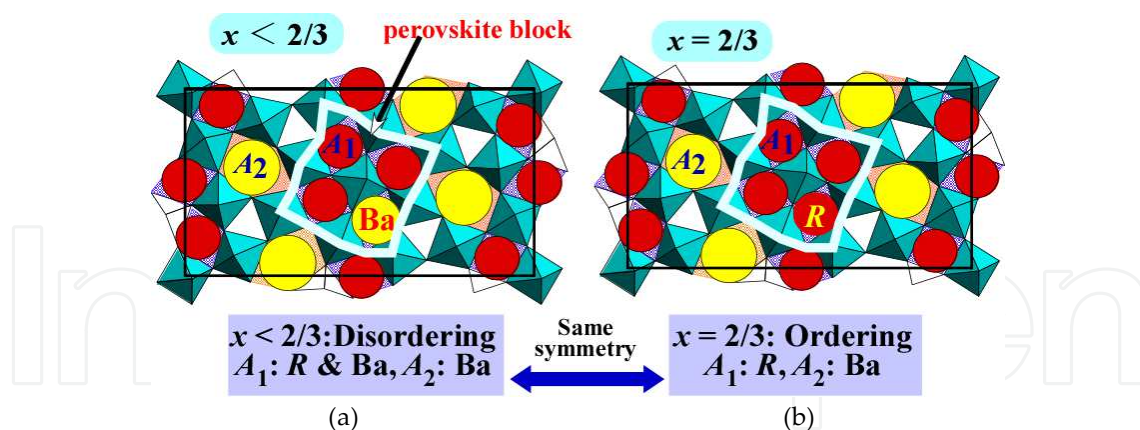


Figure 24. Crystal structure of disordering (a) and compositional ordering (b) on pseudo-tungsten-bronze solid solutions.

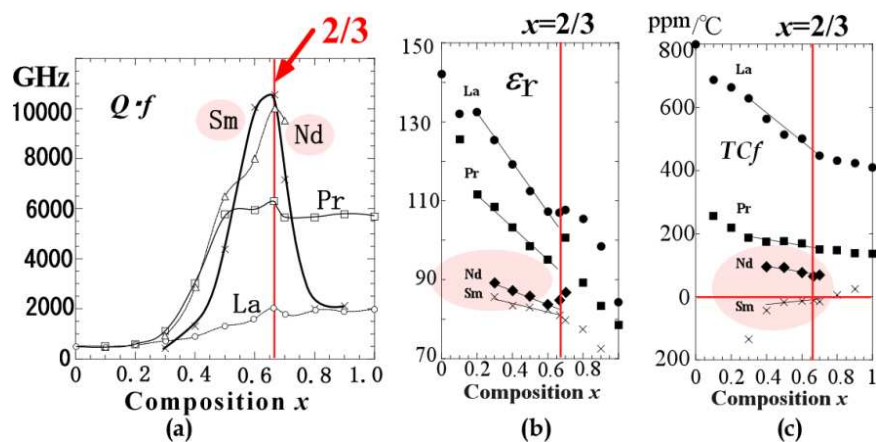


Figure 25.  $Q \cdot f$  values (a),  $\epsilon_r$  (b) and  $TCf$  (c) of pseudo-tungsten-bronze type solid solutions as a function of  $x$  in  $Ba_{6-3x}R_{8+2x}Ti_{18}O_{54}$  solid solutions.

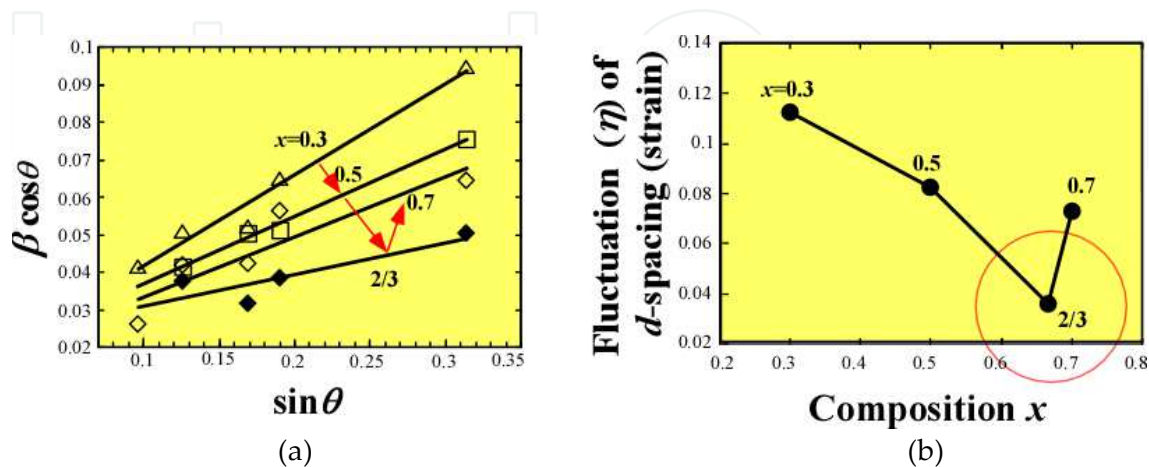


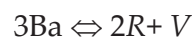
Figure 26. (a) Internal strain  $\eta$  obtained from the slope of equation  $\beta \cos \theta = \lambda/t + 2\eta \sin \theta$ . (b)

Internal strain  $\eta$  values for  $x = 0.3, 0.5, 2/3$  and  $0.7$  are shown in Fig. 26 [74]. It should be noted that the internal strain for  $x = 2/3$  is the lowest in the series of  $\text{Ba}_{6-3x}\text{Sm}_{8+2x}\text{Ti}_{18}\text{O}_{54}$  solid solutions. This low internal strain comes from the compositional ordering. As the  $x$ -values decrease according to the structural formula  $[\text{R}_{8+2x}\text{Ba}_{2-3x}\text{V}_x]_{A1}[\text{Ba}_4]_{A2}\text{Ti}_{18}\text{O}_{54}$  in the range of  $0 \leq x \leq 2/3$ , Ba ions with their larger ionic radii will also occupy a part of the rhombic sites with their smaller size. The location of Ba ions in the  $A_1$ - site leads to internal strain around the ions themselves, lowering the  $Q \cdot f$  values. Moreover, the vacancies generated in the  $A_1$ - sites by the substitution of 3Ba by 2R might be the second reason for the lowering of the internal strain and may lead to the high  $Q \cdot f$  values. On the other hand, as the  $x$ -values increase according to the structural formula  $[\text{R}_{9.33+2(x-2/3)}\text{V}_{0.66-(x-2/3)}]_{A1}[\text{Ba}_{4-3(x-2/3)}\text{V}_{3(x-2/3)}]_{A2}\text{Ti}_{18}\text{O}_{54}$  in the range of  $2/3 \leq x \leq 0.7$ , then Ba ions in pentagonal  $A_2$ - sites are substituted with vacancies and R ion occupy the vacancies in  $A_1$ - site. The decrease in Ba ions produces vacancies in  $A_2$ -sites and may lead to unstable crystal structures. Moreover, the decrease in the number of vacancies in the rhombic  $A_1$ -sites, accompanied by the decrease of Ba ions in the pentagonal sites might lead to an additional internal strain. These strains are the reason for the lower quality factor at  $x = 0.7$ . The internal strain around  $x = 0.7$  might lead to the limit of solid solutions as shown in Fig. 27 [75]. The solid solution area is different based on the R ions: the region is  $0.3 \leq x \leq 0.7$  in the case of Sm and  $0.0 \leq x \leq 0.7$  in Pr, Nd and La with inflection points at  $x = 0.2$ , which may be based on the different substitution sites.

On the other hand, the  $Q \cdot f$  values of each R analogue with  $x = 2/3$  in the  $\text{Ba}_{6-3x}\text{R}_{8+2x}\text{Ti}_{18}\text{O}_{54}$  solid solutions increase according to a decrease in the rare-earth ion size (lanthanide contraction) as shown in Fig. 28. The Sm analogue has a better  $Q \cdot f$  than the La analogue, at ca. 10,000 GHz. This crystal structure is maintained by the size difference of the cations between the Ba and R ions. It was revealed that the crystal structure with the largest size difference between Ba and Sm ions shows an excellent quality factor as it has low internal strain. On the other hand, the La analogue shows a low  $Q \cdot f$  of ca. 2,000 GHz. Though the  $Q \cdot f$  values of the Pr, Nd and Sm analogues show a linear relationship, that of the La analogue deviates from the linear relationship as shown in Fig. 28 [76]. If the changes in  $Q \cdot f$  are affected only by ionic radius, then the relationship should be linear. The reason for the deviation might be internal stress depending on the stability of the crystal structure. There are two different cation sites: the  $A_1$ - site in the perovskite block and the  $A_2$ -site in the differently sized pentagonal columns as described before, which are occupied by differently sized cations. As the difference in ionic radius between Ba and La is not large in comparison with other R ions, the crystal structure is not stable, and shows a tendency of changing toward a perovskite structure which has only a single site for large cations. So, in the case of the La-ion, the internal stress always exists as an intrinsic quality, and the internal stress might cause the deviation of  $Q \cdot f$  from the expected linear relationship. The  $\epsilon_r$  and  $TCf$  lines against ionic radius of R increase according to the increasing size of ionic radius. The parameters are not affected by the crystal structure. The reason why the  $\epsilon_r$  and  $TCf$  lines are proportional has not yet been clarified [76].

The dielectric constant  $\epsilon_r$  is affected by the following three factors: (I) volume of  $\text{TiO}_6$  octahedra; (II) tilting of octahedra strings; and (III) polarizabilities of R and Ba ions [77]. The dielectric constants  $\epsilon_r$  of the solid solutions are proportional to lattice parameters or cell volumes as

shown in Fig. 29. As  $x$  increased,  $\epsilon_r$  decreased linearly (Fig. 25(b)), and lattice parameters or cell volumes also decreased linearly (Fig. 27). Usually, in the perovskite structure, the polarity of the Ti ion in the octahedra is produced as a result of the large octahedral volume. Thus, as the mean value of the volume decreased from  $9.946 \text{ \AA}^3$  at  $x=0.5$  to  $9.925 \text{ \AA}^3$  at  $x=0.7$ , this volume change is considered to have decreased  $\epsilon_r$ . However, the volume change is very small, thus other effects should be examined such as tilting of the  $\text{TiO}_6$  octahedra strings as suggested by Valant *et al.* [78]. The tilting angle, which is that between the  $c$ -axis and the central axis of the octahedra as shown in Fig. 30, is inversely proportional to lattice parameters: the mean tilting angle is  $9.99^\circ$  at  $x=0.5$  and  $10.63^\circ$  at  $x=0.7$ , based on the refined crystal structure of the Sm solid solution series [13]. From Fig. 29, it was also deduced that the polarizabilities of  $R$  ions affect  $\epsilon_r$  and  $TCf$ . In the table of polarizabilities derived by Shannon [79], the La ion, which gives the largest  $\epsilon_r$  in the series, also has the largest polarizability among these  $R$  ions: 6.03 for La, 5.31 for Pr, 5.01 for Nd and  $4.74 \text{ \AA}^3$  for Sm. The  $\epsilon_r$  values decrease with the polarizabilities. On the other hand, the  $\epsilon_r$  values also vary linearly as a function of cell volume in each  $R$ -system as shown in Fig. 29 (a). The variations in  $\epsilon_r$  are also affected by the polarizabilities of  $R$  and Ba ions. The substitution is performed according to the following equation:



The total polarizabilities due to the substitution equation are reduced from  $3 \times 6.40$  to  $2 \times 6.03 \text{ \AA}^3$  for the La system. Here, the value of  $6.40 \text{ \AA}^3$  for the  $\text{Ba}^{+2}$  ion is larger than that for the  $\text{La}^{+3}$  ion.

The  $TCf$  is also plotted as a function of cell volume in Fig. 29 (b). Though a similar tendency to  $\epsilon_r$  is observed, the mechanism of  $TCf$  has not yet been clarified. The  $TCf$  values of the Sm system are usually negative but close to zero as shown in Fig. 25(c). As  $TCf$  obeys additional rules, we could easily get a material with  $TCf = 0 \text{ ppm}/^\circ\text{C}$ . Outstanding materials with  $TCf = 0 \text{ ppm}/^\circ\text{C}$  have been realized by adding Nd or La to Sm-systems, which are composed of a solid solution with a single phase of  $x = 2/3$  [80]. So,  $TCf$  is improved to near zero  $\text{ppm}/^\circ\text{C}$  without the degradation of the  $Q \cdot f$  value. Usually, as doped materials with different sign  $TCf$  located as secondary phase, the  $Q \cdot f$  values are degraded.

- Design of outstanding materials based on the crystal structure

In this section, some cases concerning material designs based on the crystal structure are presented. Ohsato *et al.* [72, 81] have researched the crystal structure of microwave materials and clarified the relationship between material properties and crystal structure to aid the design of new outstanding materials.

- **Case 1: Design by the distribution of cations for the improvement of properties when  $x = 0$**  [82, 83]

Sr ions are introduced in to this system, in which the ionic size is located between Ba and Sm ions. As mentioned above,  $Q \cdot f$  values of  $\text{Ba}_{6-3x}\text{R}_{8+2x}\text{Ti}_{18}\text{O}_{56}$  solid solutions have the maximum value at  $x=2/3$ . In the region  $x < 2/3$ , the structural formula of the solid solutions is  $[\text{R}_{8+2x}\text{Ba}_{2-3x}$

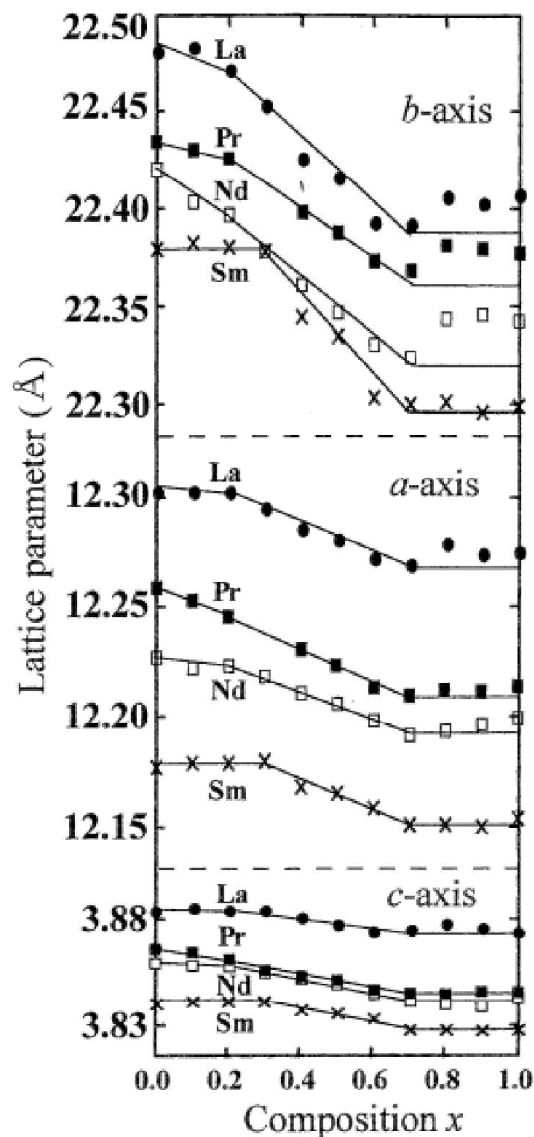


Figure 27. Lattice parameters of  $R_{6-3x}R_{8+2x}Ti_{18}O_{54}$  ( $R = La, Pr, Nd$  and  $Sm$ ) solid solutions.

$V_{x[A1]}[Ba_4]_{A2}Ti_{18}O_{54}$ . In this region, Ba ions located in  $A_1$ -sites result in a deterioration of the quality factor. In the case of  $x = 0$ ,  $Q \cdot f$  values are very low as shown in Fig. 31 (a). When Ba ions are substituted by Sr ions such as in  $[R_8Sr_2]_{A1}[Ba_4]_{A2}Ti_{18}O_{54}$ ,  $Q \cdot f$  values improved markedly from 206 to 5,880 GHz in the case of  $R = Nd$  as shown in Fig. 31 (b) [82]. The introduction of Sr ions into  $A_1$ -sites may reduce the internal strain / fluctuation of  $d$ -spacing, due to the reduction in ionic size in  $A_1$ -sites. Mercurio *et al.* [84] reported that the Sr ions occupy  $A_{13}$  special sites (Fig. 23), which have a medium size between that of  $A_1$ - and  $A_2$ -sites. Hence it is expected that  $R$ , Sr and Ba ions are ordering in  $A_1$ -,  $A_{13}$ - and  $A_2$ -sites respectively [83].

- **Case 2: Substituting Sr for Ba in  $A_1$ -sites when  $x = 0.6$**  [85]

The effects of substituting Sr for Ba in the  $A_1$ -sites of  $Ba_{6-3x}Sm_{8+2x}Ti_{18}O_{54}$  solid solutions were studied in terms of the lattice parameters and microwave dielectric properties as shown in

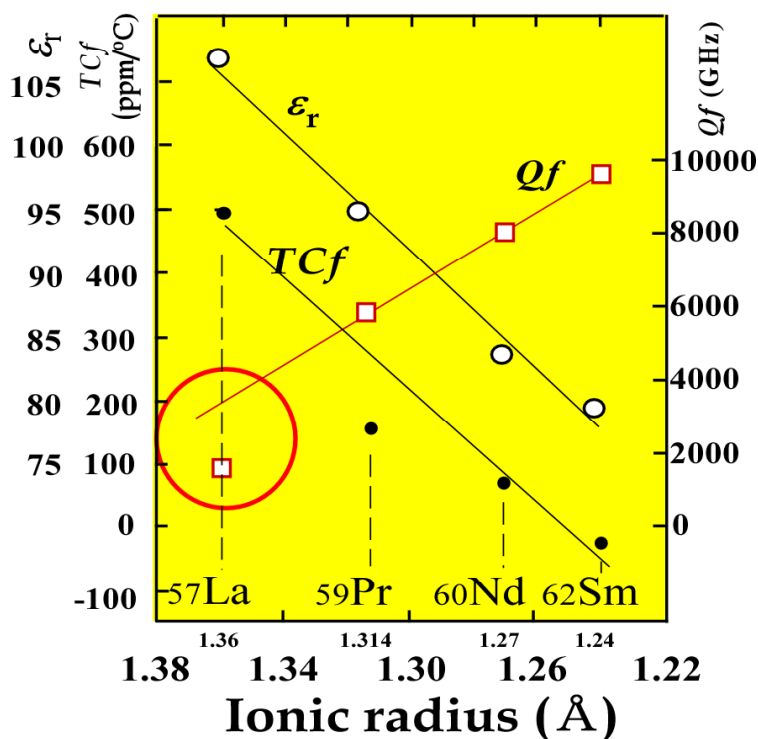


Figure 28. Microwave dielectrics properties as a function of ionic radius of R ion.

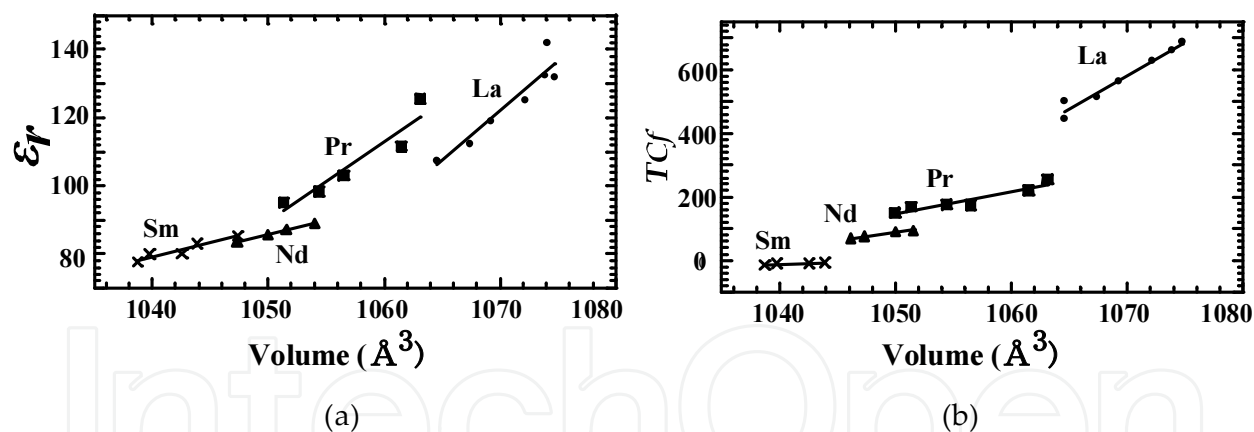


Figure 29.  $\epsilon_r$  (a) and  $TC_f$  (b) are shown as a function of unit cell volume.

Figs 32 and 33 respectively [85]. The compositions of the compounds in which Sr is substituted for Ba are as follows:  $x$  in  $(Ba_{1-\alpha}Sr_\alpha)_{6-3x}Sm_{8+2x}Ti_{18}O_{54}$  is fixed at 0.6, at which point the  $Ba_{6-3x}Sm_{8+2x}Ti_{18}O_{54}$  solid solution has excellent properties, and composition  $\alpha$ , in which Sr is substituted for Ba, ranges from 0.0 to 0.2. The properties are concerned with the strain in the crystal structure due to Sr substitution. We derived a structural formula  $[Sm_{8+2x}Ba_{2-3x}]_{A1}[Ba_4]_{A2}Ti_{18}O_{54}$  in the range  $0 \leq x \leq 2/3$  and another  $[Sm_{9.33+2(x-2/3)}]_{A1}[Ba_{4-3(x-2/3)}]_{A2}Ti_{18}O_{54}$  in the range  $2/3 \leq x \leq 1$ . In the composition  $x = 0.6$ , the formula is  $[Sm_{9.2}Ba_{0.2}]_{A1}[Ba_4]_{A2}Ti_{18}O_{54}$  which includes four Ba ions in  $A_2$ -sites on the pentagonal columns,

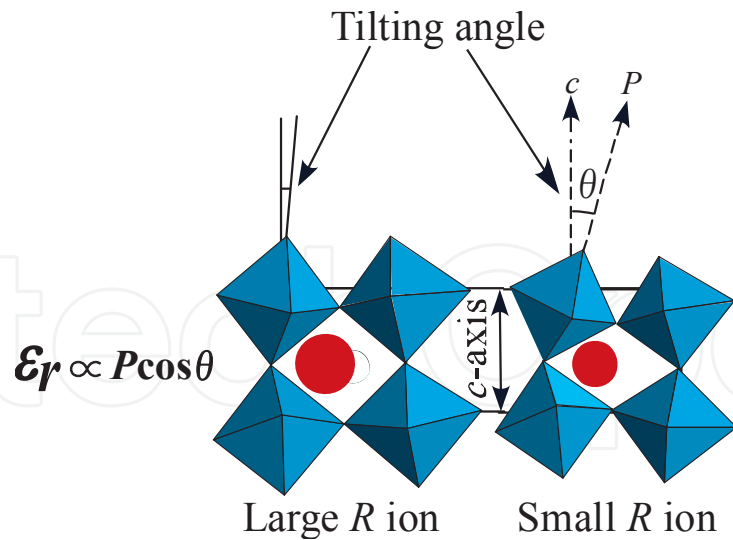


Figure 30. Correlation between dielectric constant and the tilting angle of the octahedral.

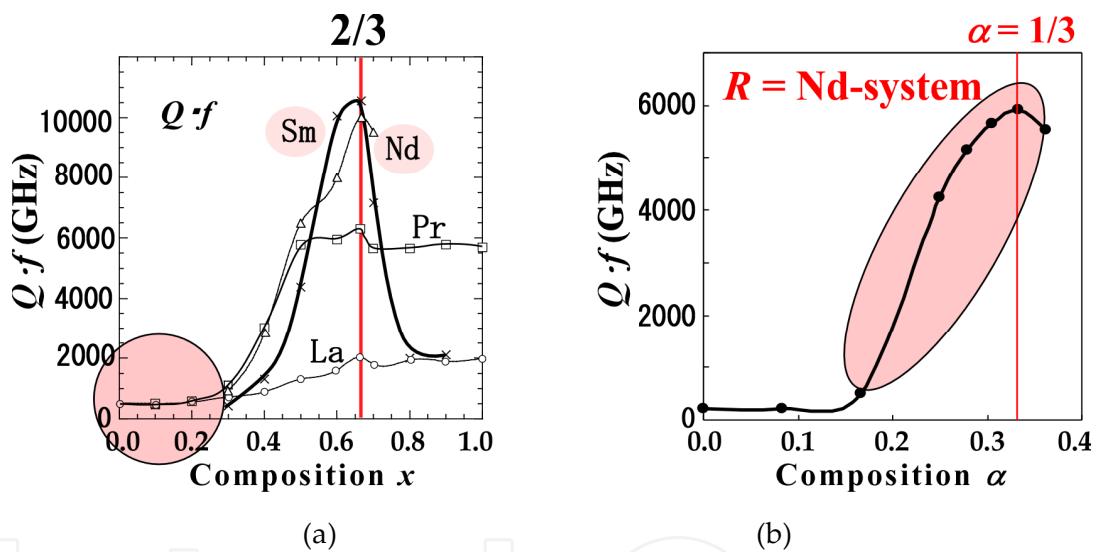


Figure 31. (a) Low  $Q \cdot f$  around  $x = 0$  on the  $Q \cdot f$  composition figure. (b)  $Q \cdot f$  values of Nd-system with  $x = 0$  improved from 200 to 6000 GHz by substitution Sr for Ba.

and 0.2 Ba ions in  $A_1$ -sites on the perovskite blocks with 9.2 Sm. The 0.2 Ba ions in  $A_1$ -sites produce the internal strain because the size of the Ba ions is fairly large for the  $A_1$ -sites. When 0.2 Ba ions are completely substituted by Sr ions, then the  $Q \cdot f$  values improve to 10,205 GHz, which shows that the strain in the crystal structure has relaxed somewhat. The composition in which Sr is substituted for 0.2 Ba is  $\alpha = 0.048$  in the  $(\text{Ba}_{1-\alpha}\text{Sr}_\alpha)_{6-3x}\text{Sm}_{8+2x}\text{Ti}_{18}\text{O}_{54}$  substitutional formula. The dielectric properties depend on the lattice parameters, the values of which change at the composition  $\alpha = 0.048$  due to the change in the substitution mode of the Sr ions. The temperature coefficient of the resonate frequency  $TCf$  was changed in the same manner as the dielectric constant [86].

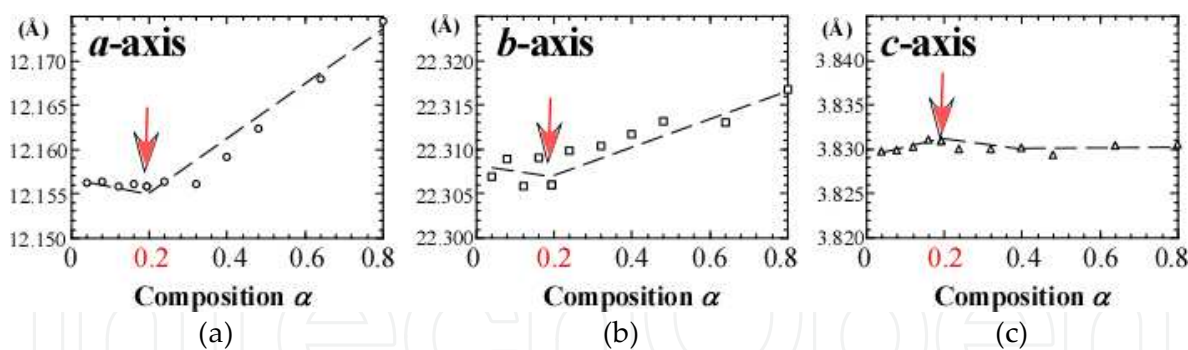


Figure 32. Lattice parameters of  $(\text{Ba}_{1-\alpha}\text{Sr}_{\alpha})_{4.2}\text{Sm}_{9.2}\text{Ti}_{18}\text{O}_{54}$  solid solutions.

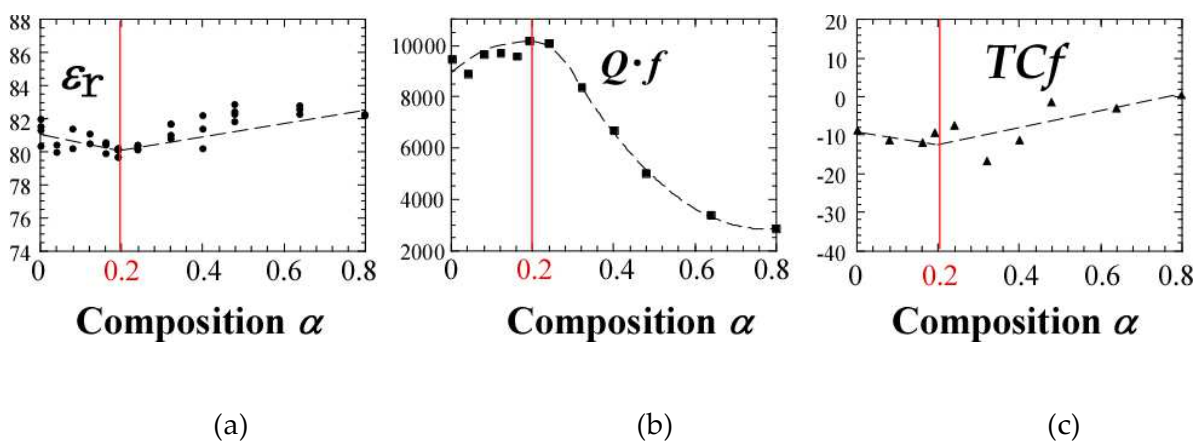


Figure 33. Microwave dielectric properties  $\epsilon_r$  (a),  $Q \cdot f$  (b) and  $TCf$  (c) of  $(\text{Ba}_{1-\alpha}\text{Sr}_{\alpha})_{4.2}\text{Sm}_{9.2}\text{Ti}_{18}\text{O}_{54}$  solid solutions as a function of composition  $\alpha$ .

### 3.2.2. Homologous compounds with perovskite layered structure

There are three kinds of homologous series composed of a perovskite layered structure. The perovskite layers have three different orientations such as (111) the plane series for  $\text{Ba}_n\text{La}_4\text{Ti}_{3+n}\text{O}_{12+3n}$  (100) the series for the Ruddlesden-Popper phase and (110) the series for  $\text{A}_n\text{B}_n\text{O}_{3n+2}$  homologous compounds as shown in Tables 2(h)–(j). [87, 88]

#### • (111) series for $\text{Ba}_n\text{La}_4\text{Ti}_{3+n}\text{O}_{12+3n}$ homologous compounds

The homologous compounds are also perovskite related compounds composed of a layered structure. The compounds are located in a  $\text{R}_2\text{O}_3$ -rich region, compared to pseudo-tungsten-bronze solid solutions in the  $\text{BaO}-\text{RO}_3-\text{TiO}_2$  ternary phase diagram as shown in Fig. 22. The chemical formula is shown as  $\text{Ba}_n\text{La}_4\text{Ti}_{3+n}\text{O}_{12+3n}$  and there are four compounds at intervals  $n = 0, 1, 2,$  and  $4$  as shown in Fig. 34 [89–92]. As a compound with  $n = 4$  is unstable below  $1,450^\circ\text{C}$ , other compounds where  $n = 0, 1$  and  $2$  are studied in this paper [93–97]. In particular, we mainly synthesized two compounds of  $n = 1$  and  $2$ . These compounds,  $n = 0$ :  $\text{La}_4\text{Ti}_3\text{O}_{12}$  (2:3),  $n = 1$ :  $\text{BaLa}_4\text{Ti}_4\text{O}_{15}$  (1:2:4), and  $n = 2$ :  $\text{Ba}_2\text{La}_4\text{Ti}_5\text{O}_{18}$  (2:2:5), show hexagonal layered perovskite struc-

tures as shown in Fig. 35 [89]. Another  $R$  ion included in this homologous compound is the Nd ion, and the alkali earth ions Ca and Sr, substituted for Ba.

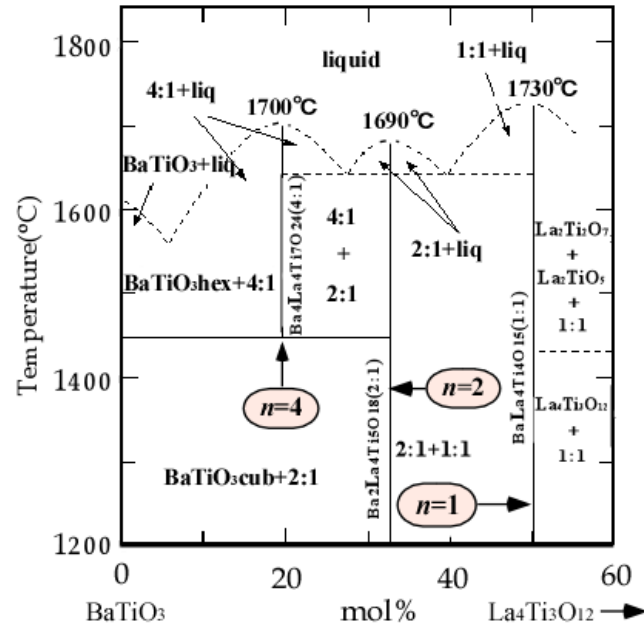


Figure 34. Binary phase diagram for  $Ba_nLa_4Ti_{3+n}O_{12+3n}$  homologous compounds.

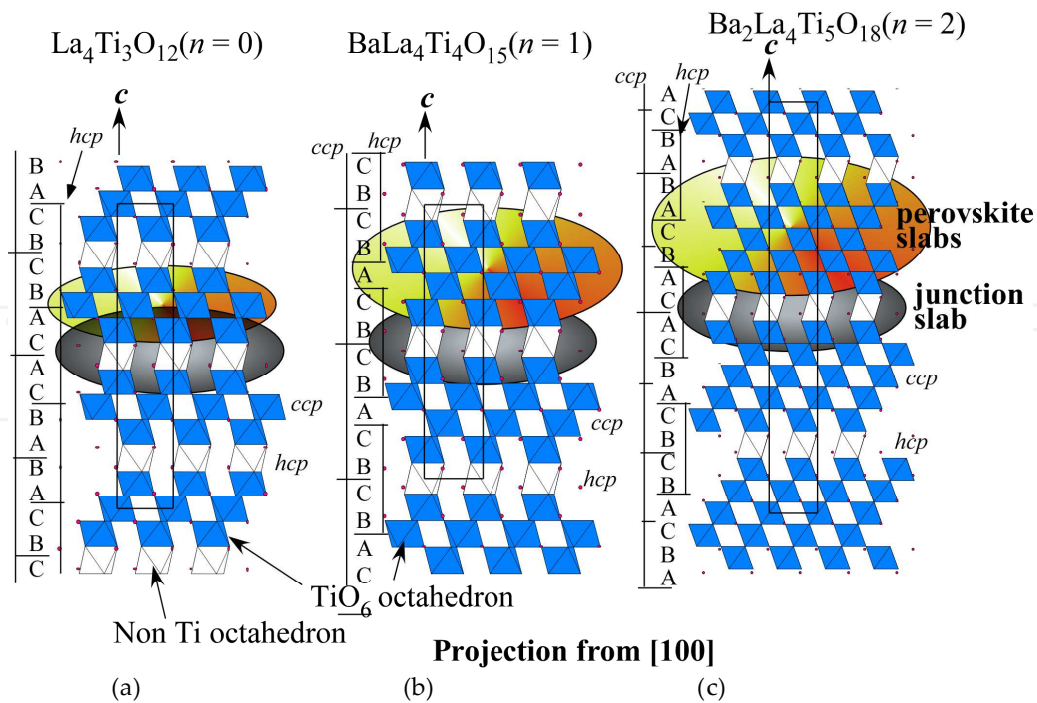
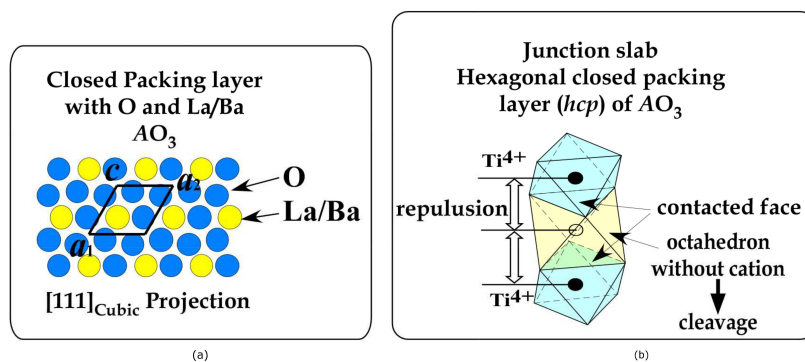
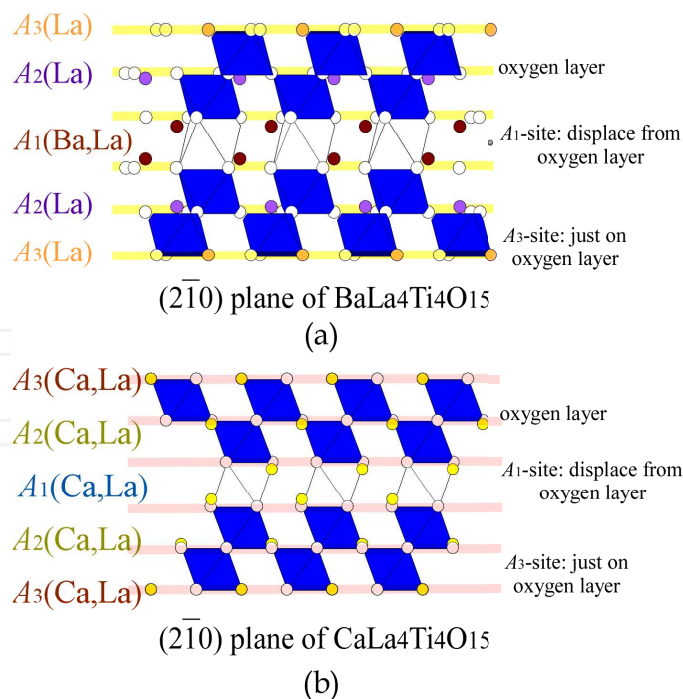


Figure 35. Crystal structure of  $Ba_nLa_4Ti_{3+n}O_{12+3n}$  homologous compounds (a)  $La_4Ti_3O_{12}$  ( $n = 0$ ), (b)  $BaLa_4Ti_4O_{15}$  ( $n = 1$ ), and (c)  $Ba_2La_4Ti_5O_{18}$  ( $n = 2$ ).



**Figure 36.** (a) Closed packing layer composed by oxygen and La/Ba atoms, which is one of specific features, (b) Junction slab composed by octahedron. Cleavage easily occurs at the center octahedron without cation.

The crystal structure of homologous  $BaLa_4Ti_4O_{15}$  ( $n = 1$ ) compounds is illustrated in Fig. 35(b). The crystal data are trigonal,  $P\bar{3}c1$  (No. 165) and  $Z = 2$ . This compound has a sequence of five layers with La/BaO<sub>3</sub> closed packing as shown in Fig. 36 (a), like *hccch* of the  $Ba_5Nb_4O_{15}$  type. Here, Ba is the cation located in the cuboctahedron of the perovskite structure, where *h* means hexagonal close packing (*hcp*) and *c* is cubic close packing (*ccp*). The perovskite slab with *ccp* is composed of four  $TiO_6$  octahedral layers and the junction slab with *hcp* between perovskite slabs is composed of a three-octahedron string shared face with an empty octahedron in the center as shown in Fig. 36 (b).



**Figure 37.** Alkaline earth elements in the  $A_1$ ,  $A_2$ , and  $A_3$ -sites in the closed packing layer of  $BaLa_4Ti_4O_{15}$  (a) and  $CaLa_4Ti_4O_{15}$  (b) viewed along  $(2\bar{1}0)$ . Ba ions with a large ionic radius are located only in  $A_1$ -sites of Ba analogues, while on the other hand, Ca ions of Ca analogues are distributed across all sites with La ions.

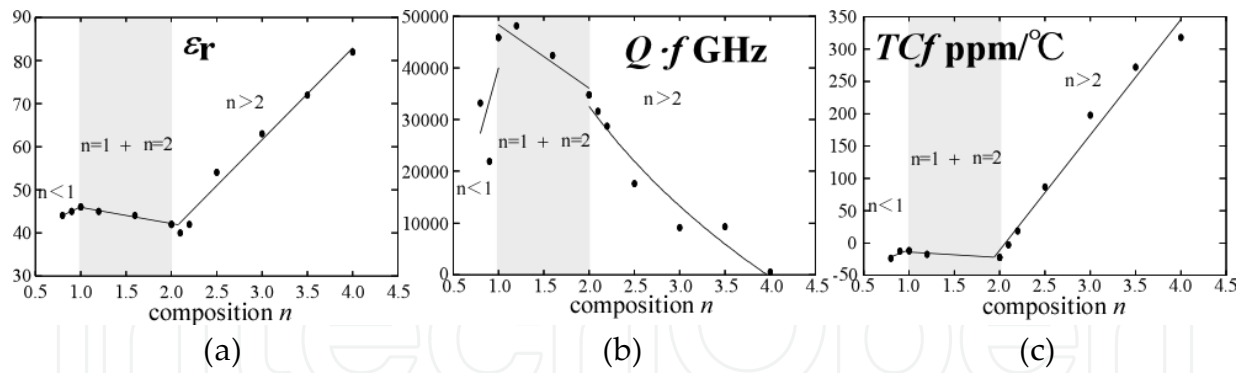


**Figure 38.** Microwave dielectric properties of  $\text{Ba}_n\text{La}_4\text{Ti}_{3+n}\text{O}_{12+3n}$  ceramics as a function of the composition  $n$ .

A	Sintering condition	$D_r$ (%)	$\epsilon_r$	$Q \cdot f$ (GHz)	$TCf$ (ppm/°C)
Ba	1600°C 2 h	98.4	44.4	41,008	-26
Sr	1550°C 48 h	98.9	43.7	46,220	-8.4
Ca	1550°C 24 h	94.8	41.1	50,246	-25.5

**Table 4.** Relative density and microwave dielectric properties of  $\text{ALa}_4\text{Ti}_4\text{O}_{15}$  ( $A=\text{Ba}$ ,  $\text{Sr}$  and  $\text{Ca}$ ).

The compound can include Sr and Ca ions substituted in place of Ba ions. The homologous  $\text{ALa}_4\text{Ti}_4\text{O}_{15}$  ( $A = \text{Ba}$ ,  $\text{Sr}$ , or  $\text{Ca}$ ) compounds have a different ordering for  $A$ -site cations as shown in Fig. 37. In the case of Ba analogues, the ordering of Ba ( $r = 1.61 \text{ \AA}$ ) and La ions ( $r = 1.36 \text{ \AA}$ ) will occur as follows: Ba ions located in  $A_1$ -sites near the junction slab, and La ions in all  $A_1$ ,  $A_2$  and  $A_3$ -sites as shown in Fig. 37 (a) [96]. In the case of Sr and Ca analogues, the Sr ions ( $r = 1.44 \text{ \AA}$ ) and the Ca ions ( $r = 1.34 \text{ \AA}$ ) are all located in  $A$ -sites including La ions as shown in Fig. 37(b). As the space of  $A_1$ -sites is larger than those of  $A_2$ - and  $A_3$ -sites,  $\text{Ba}^{2+}$  ions with their large ionic radii predominantly occupy  $A_1$ -sites. On the other hand, as the ionic radii of Sr and  $\text{Ca}^{2+}$  are close to that of  $\text{La}^{3+}$  ions, the Sr and the Ca ions of the Sr and Ca analogues randomly occupy the  $A$ -sites [96].

The microwave dielectric properties of  $\text{Ba}_n\text{La}_4\text{Ti}_{3+n}\text{O}_{12+3n}$  are shown in Fig. 38 as functions of composition [93]. The sample with the composition  $n = 1$  shows the best properties, such as the highest  $Q \cdot f = 46,000 \text{ GHz}$ ,  $\epsilon_r = 46$ , and  $TCf = -11 \text{ ppm/}^\circ\text{C}$ , which can be improved to near zero  $\text{ppm/}^\circ\text{C}$  by means of the substitution of Al for La [94]. The microwave dielectric properties of the Ba, Sr, and Ca analogue ceramics are shown in Table 4 [97]. These samples showed excellent microwave dielectric properties for use in base stations of mobile phones, such as a value of  $\epsilon_r$  greater than 40, a  $Q \cdot f$  greater than 40,000 GHz and a  $TCf$  within  $\pm 30 \text{ ppm/}^\circ\text{C}$ . The highest  $\epsilon_r$  of 44.4 was observed in the case of the Ba analogue and the value decreased to 41.1 for Ca. The highest  $Q \cdot f$  of 50,246 GHz was observed in the case of the Ca analogue, and the value decreased to 46,220 GHz for Sr and to 41,008 GHz for Ba. These values are much higher than those in an earlier report.

We would like to consider the reason for the large  $\epsilon_r$  and the high  $Q \cdot f$  based on the crystal structure. There are three characteristic points of the crystal structure: one is the size of the cation sites, another is the shift of the cation positions, and the third is the different divalent cation distributions. The large volume of cation sites results in the large  $\epsilon_r$ . Divalent cation  $A$  with a large ionic radius, such as Ba, Ca and Sr, expands the lattice and brings an enlargement of cation sites. In particular, the expansion of the  $B$ -site volume affects Ti ion movement as a result of the rattling effect. In the case of the Ba analogue with the highest  $\epsilon_r$  value, the volume is larger than that of the Ca analogue. The Ba ion with its large ionic radius of 1.61 Å is more effective than the Ca ion with  $r = 1.34$  Å. In the second case of the shift of the cation positions, the  $\epsilon_r$  of the Ba analogue with a large shift is larger than that of the Ca analogue. This shift might increase the movability of the La ion with a small ionic radius, so that the  $\epsilon_r$  of the Ba analogue with a large shift is greater than that of the Ca analogue. The high  $Q \cdot f$  value might come from the cation distribution and the volume of cation sites. In the case of the Ca analogue, as the shift of cations from the close packed layer of oxygen is smaller than it is for Ba analogue, then widely occupied  $A$ -sites might be distributed periodically with La ions to bring a high  $Q \cdot f$ . The  $\epsilon_r$  values also depend on the ionic polarizations of Ba ( $P = 6.4$ ), Sr ( $P = 4.24$ ), and Ca ( $P = 3.16$ ) [97]. These homologous compounds show characteristic near-zero ppm/°C values of the  $TCf$ . The  $TCf$  of the Sr analogue is near zero ppm/°C compared with that of the others, whose might come from the analogue of SrTiO<sub>3</sub> having a large positive  $TCf$  of 1,200 ppm/°C. Moreover, the  $TCf$  of the Ba analogue was improved to a near zero 1.3 ppm/°C, with a high  $\epsilon_r$  of 44 and a  $Q \cdot f$  of 47,000 GHz by substituting Al ions for La ions [97].

- **(100) series for Ruddlesden-Popper phase**

The Ruddlesden-Popper phase [98, 99] is shown with the chemical formula  $A_{n+1}B_nO_{3n+1}$ . Here,  $A$  is a cuboctahedral site and  $B$  is an octahedral site. These space groups are all  $I4/mmm$  (No. 139) with a center of symmetry  $i$ . The phase is composed of SrTiO<sub>3</sub> layers with (100)<sub>cubic</sub> plane as shown in Fig. 39(a). The layers are stacked, shifting each other by  $(1/2a, 1/2b)$ . Among the layers, a SrO halite type structure is formed. The chemical formula is shown as  $AO \cdot n(ABO_3)$ . Here,  $n = 1$ : Sr<sub>2</sub>TiO<sub>4</sub> [98] is K<sub>2</sub>NiF<sub>4</sub> type stacking of one  $ABO_3$  and three unit cells of perovskite;  $n = 2$ : Sr<sub>3</sub>Ti<sub>2</sub>O<sub>7</sub> is the stacking of two  $ABO_3$  similar to  $n = 1$ ,  $n = 3$ : Sr<sub>4</sub>Ti<sub>3</sub>O<sub>10</sub> is also the stacking of three  $ABO_3$  with (100). CaSmAlO<sub>4</sub> ceramics with a K<sub>2</sub>NiF<sub>4</sub> crystal structure are presented as microwave dielectrics [100]. The microwave dielectric properties are shown in Table 2 (i). Although the Aurivillius phase  $A_{n+1}B_nO_{3n+3}$  [101, 102] and the Dion-Jacobson phase  $M^+ [Ca_2Na_{n-3}Nb_nO_{3n+1}]$  exist in addition to the Ruddlesden-Popper phase in the (100) series [103,104], the microwave dielectric properties are not presented.

- **(110) series for  $A_nB_nO_{3n+2}$  homologous compounds**

A (110) planar perovskite layered structure also creates a homologous series of  $A_nB_nO_{3n+2}$ . A typical example of this series is Sr<sub>2</sub>Ta<sub>2</sub>O<sub>7</sub> with  $n = 4$  as shown in Fig. 39 (b) [105, 106]. The value of  $n$  is that of the octahedral layer in the single perovskite layer as seen in the figures. The layered structure was formed by the addition of oxygen atoms to non-bridged oxygen atoms of the  $BO_6$  octahedron cut. The microwave dielectric properties are also shown in Table 2 (j).

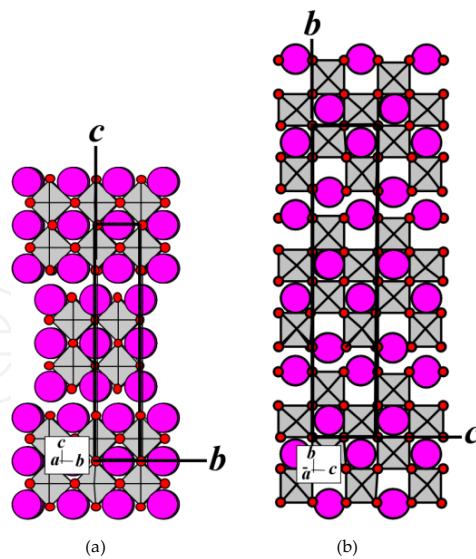


**Figure 39.** Crystal structure of layered perovskite: (a) (100) series: Ruddlesden-Popper phase of  $\text{Sr}_3\text{Ti}_2\text{O}_7$  ( $n = 2$ ), and (b) (110) series:  $A_nB_n\text{O}_{3n+2}$  homologous compound of  $\text{Sr}_2\text{Ta}_2\text{O}_7$  ( $n = 4$ ).

#### • Application of perovskite related compounds

These perovskite related compounds are applied to microwave dielectrics. Dr. Okawa studied pseudo-tungsten-bronze solid solutions and (111) plane homologous series in his doctoral thesis [108], and these materials have been used in microwave applications. Microwave dielectrics based on  $\text{Ba}_4(\text{R}_{1-y}\text{Bi}_y)_{9+1/3}\text{Ti}_{18}\text{O}_{54}$  ( $R$ : rare earth) solid solutions with Bi partially substituted for  $R$  were clarified with a high  $\epsilon_r$  of  $> 80$  [109,110]. They are used widely in the wireless communication systems of fire engines in Japan. An Al doped  $\text{BaLa}_4\text{Ti}_4\text{O}_{15}$  homologous compound, which has the best microwave dielectric properties for use as a resonator was developed for use in the base stations of wireless communication systems [94]. It is currently used in base stations of the mobile communication systems of the Tokyo metro. In addition, at near  $n = 0$  in  $\text{Ba}_n\text{La}_4\text{Ti}_{3+n}\text{O}_{12+3n}$  homologous compounds, a superior material was developed with properties of  $\epsilon_r = 42$ ,  $Q \cdot f = 86,000$  GHz, and  $TCf = -17$  ppm/ $^\circ\text{C}$  [111, 112].

## 4. Flexibility of perovskite structure and microwave dielectric properties

As already described in many parts of this book, the structure of perovskite is flexible, producing many specific phases such as ferroelectrics and paraelectrics. This flexibility is due to the inclusion of many cations in the perovskite structure. There are three important features of the perovskite structure, detailed below :

- The first is the framework of octahedra connecting all their apexes with each other in three dimensions.
- The second is the closed packing layer of  $\text{AO}_3$  instead of oxygen closed packing as shown in Fig. 36 (a).

- The third important feature is the large cation site, that is, cuboctahedron with basically 12 coordination.

The first produces two spaces for cations — octahedron and cuboctahedron — described as the third feature above, which many kinds of cations with different ionic radii and electric charges can occupy. This framework will be deformed and tilting. These features produce many kinds of ferroelectric and paraelectric properties. The closed packing of  $AO_3$  discussed as the second feature of the perovskite structure, produces a high density, as heavy  $A$  ions are incorporated in the layer instead of oxygen. These high density and heavy materials are found in high pressure environments such as the deeper parts of the earth [113]. The cuboctahedron points are produced by connecting the  $AO_3$  packing layer with  $B$  ions. This polyhedron includes special large cations such as Ba, Ca and Sr. If smaller sized ions such as Mg are present, the crystal structure formed will be that of ilmenite, similar to the  $Al_2O_3$ -type.

Furthermore, the flexibility of the perovskite structure is shown by the fact that different sized plural large cations can be also included in the deformed crystal structure. There are some examples as follows:

- Example 1: In the case of the order-disorder transition in complex perovskite, when the structure is ordered, two different sites appear under the changing crystal structure form from cubic to trigonal [38] as shown in Fig. 11.
- Example 2: As in the case of  $SrTiO_3$  doped  $LaAlO_3$ , the structure creates a site partially occupied with Ti-ions under the space group change from  $R\bar{3}c$  to  $R\bar{3}$  [35, 36]. The crystal changes bring an improvement in  $Q \cdot f$  due to a decrease in internal strain.
- Example 3: Although these examples do not change the framework of the perovskite structure, if the size difference becomes large enough, then the framework could be changed such as in the tungsten-bronze structure described above. In the case of tetragonal tungsten-bronze with a simple structure, the crystal structure change is illustrated in Fig. 40 [114]. When a perovskite block rotates slightly, the structure produces a pentagonal and a trigonal site from two cuboctahedra. Contrary, if the two different sized ions become the same size in the tungsten-bronze structure, then the crystal structure becomes a perovskite structure. In the case of pseudo-tungsten-bronze solid solutions, as the size difference between the Ba and La ions is small and causes the strain, the dielectric losses increase as described above (Fig. 28) [76].

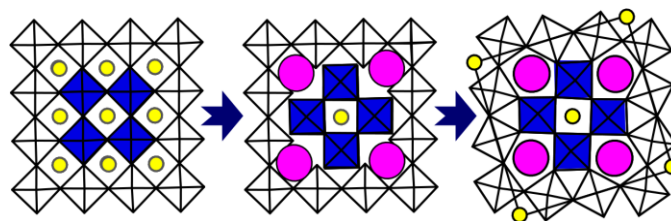


**Figure 40.** The structure of perovskite changes to a tungsten-bronze structure after the inclusion of two differently sized large ions, producing rhombic ( $A_1$ ) and pentagonal ( $A_2$ ) sites.

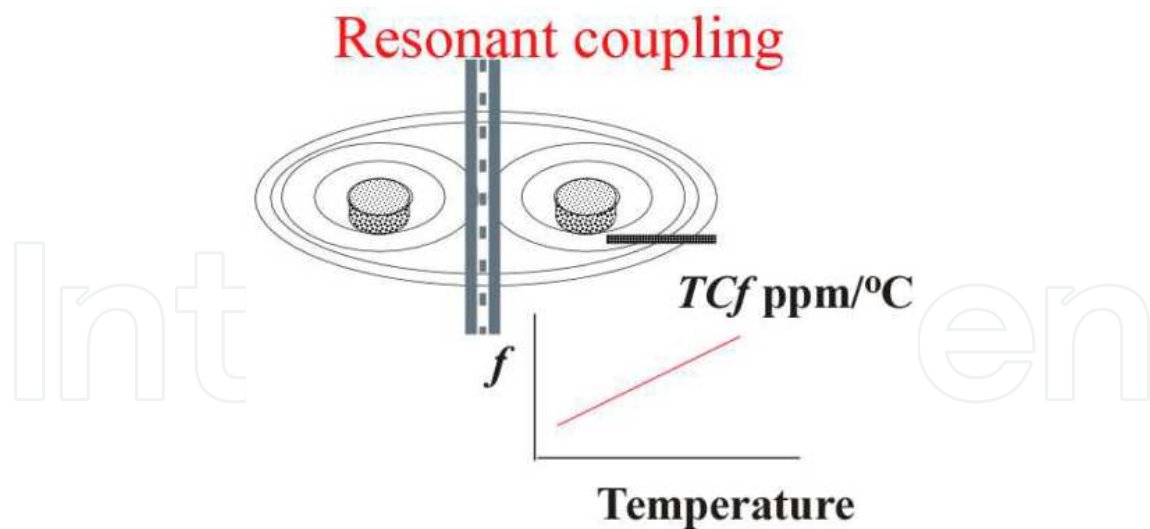


**Figure 41.** Resonant coupling for the temperature measurement of isolated places.

The intrinsic reasons for the ordering and symmetry effects on  $Q \cdot f$  properties are that ordering reduces the internal stress and high symmetry reduces the formation of poles. Which effect is predominant? As described above, in the absence of phase transition such as in pseudotungsten-bronze solid solutions, compositional ordering is predominant [74]. In the case of complex perovskite with an order-disorder transition, high symmetry is predominant rather than ordering, as described above [58, 65].

## 5. Functional advances in the next generation of microwave dielectrics

In this section, the future large scale application of microwave dielectrics will utilize some new and novel functions — based on microwave properties — as follows:

- (1) electromagnetic resonance,
- (2) electromagnetic wave shortening,
- (3) electromagnetic wave delay,
- (4) temperature variation of resonant frequency,
- (5) electromagnetic wave absorption
- (6) other functions such as transparency and refractive index.

As the content has been published in both “*A Handbook of Multifunctional Ceramics*” [17] and a paper [115], please refer to those publications. Some important functions are presented below.

Fig. 41 shows a type of temperature sensor utilizing resonant coupling, which can measure the temperature on the opposite side of a wall without the need for an electric wire. The materials should have an extremely large  $TCf$  depending on the temperature. Fig. 42 shows a well-known

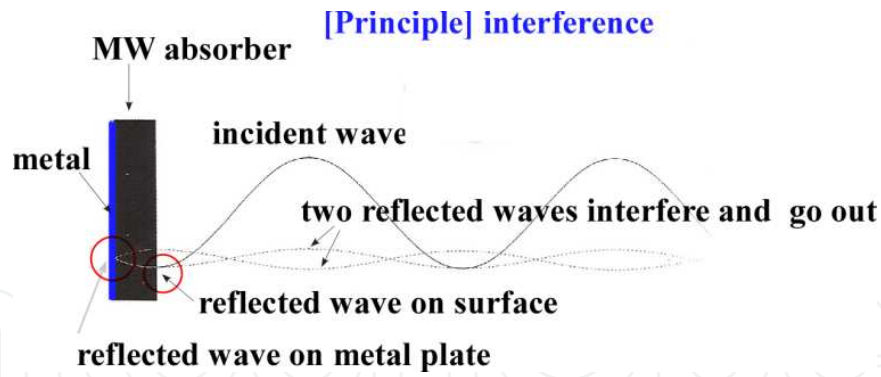


Figure 42. Principle of electromagnetic wave absorber.

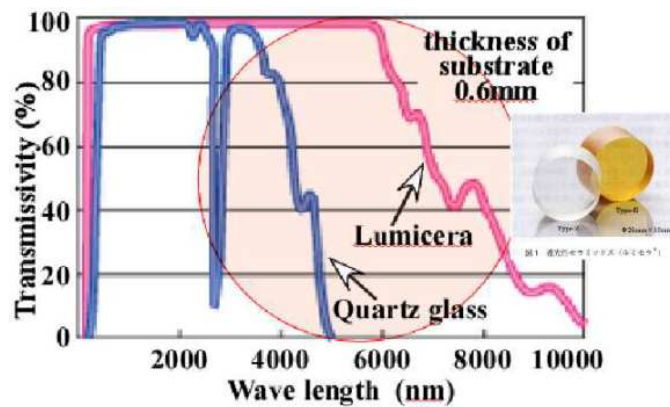


Figure 43. Transmissivity of Lumicera compared with quartz glass. Transparent region expanded to middle IR region.

principle of an electromagnetic wave absorber in a good design using wave interference, dielectric losses and wave retardation in the materials [116]. As in this example, new functions will be derived from the properties of the materials, and from physical principles. Fig. 43 shows the extreme transparency ceramics of Lumicera produced by Murata Manufacturing Co., Ltd. in Japan [117]. These materials are also microwave dielectrics, such as BMT — the ‘king’ of microwave dielectrics — as described above. The fabrication technology takes full advantage of our current understanding of the materials, such as controlled to cubic phase without birefringence.

## 6. Conclusion

Many kinds of microwave dielectrics with perovskite and related structure have been produced based on research into the relationship between the crystal structure and its properties. In this chapter, the following compounds related perovskite are introduced and discussed: simple perovskite, complex perovskite, pseudo-tungsten-bronze solid solutions and layered perovskite compounds such as  $Ba_nLa_4Ti_{3+n}O_{12+3n}$  homologous with (111), Ruddlesden-Popper phase with (100) and  $A_nB_nO_{3n+2}$  homologous with (110) oriented perovskite layers. Most of these

compounds are paraelectrics with a center of symmetry  $i$ , and include many types of ion with different ionic radii and electric charges. They are also designed using stoichiometric techniques to develop superior properties. The superior microwave materials developed should be utilized in new and useful applications for the benefit of future generations.

## Acknowledgements

I would like to thank Professors and graduate students of NIT, Meijo University and Hoseo University, and Doctors and researchers in the many companies which collaborated with NIT. A part of this work was supported by the following projects: (1) Support industries of Japan by Ministry of Economy, Trade and Industry (METI), Japan. (2) MEXT/JSPS KAKENHI Grant Number 25420721. (3) Adaptable & Seamless Technology Transfer Program (A-step) by MEXT, Japan

## Author details

Hitoshi Ohsato<sup>1,2\*</sup>

Address all correspondence to: ohsato.hitoshi@nitech.ac.jp

1 Nagoya Industrial Science Research Institute, Nagoya, Japan

2 Nagoya Institute of Technology, Nagoya, Japan

## References

- [1] Sebastian MT. Dielectric Materials for Wireless Communication. Amsterdam: Elsevier. 2008; ISBN-13:978-0-08-045330-9
- [2] Sebastian MT, Uvic R, Jantunen H. Low-loss dielectric ceramic materials and their properties. *International Materials Review*. 2015;60:395-415.
- [3] Ohsato H. High frequency dielectric ceramics. in: Adachi G editor. *Materials Technology Hand Book for Rare-earth Elements*. Tokyo: NTS Inc; 2008. p. 346–358. (Japanese).
- [4] Ohsato H, Kagomiya I, Chae KW. Microwave dielectric ceramics with rare-earth elements (I). *J Korean Phys Soc*. 2012;61:971-979.
- [5] Ohsato H, Kagomiya I, Kim JS. Microwave Dielectric Ceramics with Rare-Earth (II). *Integrated Ferroelectrics*. 2010;115:95-109.

- [6] Wakino K. Recent Development of Dielectric Resonator Materials and Filters in Japan. *Ferroelectrics*. 1989;91:69-86.
- [7] Tamura H. Progress of Ceramic Dielectric Materials for Microwave and Millimeter-wave Applications. *MWE '99 Microwave Workshop Digest*. 1999; p. 175-180.
- [8] Kobayashi Y, Katoh M. Microwave Measurement of Dielectric Properties of Low-loss Materials by the Dielectric Resonator Method. *IEEE Trans. on MTT*. 1985;MTT-33:586-92.
- [9] Ichinose N. High-frequency materials and their applications. In: *New Ceramics & Electronic Ceramics*. 1996;9(9):p. 1-50.
- [10] Ohsato H, Ohhashi T, Kato H, Nishigaki S, Okuda T. Microwave Dielectric Properties and Structure of the  $\text{Ba}_{6-3x}\text{Sm}_{8+2x}\text{Ti}_{18}\text{O}_{54}$  Solid Solutions. *Jpn J Appl Phys*. 1995;34:187-191.
- [11] Ohsato H. High Frequency Dielectrics. In: Shiosaki T, editor. *Development and Applications of Ferroelectric Materials*. CMC; 2001. p. 135-147 (Japanese).
- [12] Ohsato H. Development for Microwave dielectric ceramics. *JCLS*. 2003;55:1207-1218.
- [13] Ohsato H. Research and Development of Microwave Dielectric Ceramics for Wireless Communications. *J Ceram Soc Jpn*. 2005;113:703-711.
- [14] Ohsato H. New frontiers of microwave dielectrics with perovskite-type structure. *Bulletin Japan Ceramics Society*. 2008;43:597-609 (Japanese).
- [15] Ohsato H. Research and Development for Electroceramics Based on Crystal Structure. In: *Proceedings of the 4th Fulrath Memorial International Symposium on Advanced Ceramics*; 4 April 2007; Tokyo; 2007. p. 1-6.
- [16] Ohsato H. Design of Microwave Dielectrics Based on Crystallography. In: Akedo J, Chen XM, Tseng T, editors. *Advances in Multifunctional Materials and Systems II*, In: *Ceramic Transactions*. John Wiley & Sons; 2014;245:87-100.
- [17] Ohsato H, Microwave dielectrics. In: Fukunaga O, Haneda H, Makishima A, editors. *Handbook of Multifunctional Ceramics*. Tokyo: NTS; 2011. P.152-166 (Japanese).
- [18] Kajfez D, Guillon P, *Dielectric resonators*. 2<sup>nd</sup> ed. Atlanta: Noble Publishing Corporation; 1998.
- [19] Ohsato H. Microwave Materials with High Q and Low Dielectric Constant for Wireless Communications. *Mater Res Soc. Symp. Proc*. 2005;833:55-62.
- [20] Tsunooka T, Andou M, Higashida Y, Sugiura H, Ohsato H. Effects of  $\text{TiO}_2$  on sinterability and dielectric properties of high-Q forsterite ceramics. *J Eur Ceram Soc*. 2003;23:2573-2578.

- [21] Tsunooka T, Sugiyama H, Kakimoto K, Ohsato H, Ogawa H. Zero Temperature Coefficient  $\tau_f$  and Sinterability of Forsterite Ceramics by Rutile Addition. *J Ceram Soc Jpn Suppl.* 2004;112:S1637-S1640.
- [22] Guo Y, Ohsato H, Kakimoto K. Characterization and dielectric behavior of willemite and TiO<sub>2</sub>-doped willemite ceramics at millimeter-wave frequency. *J Eur Ceram Soc.* 2006;26:1827-1830.
- [23] Surendran KP, Santha N, Mohanan P, Sebastian M. Temperature stable low loss ceramic dielectrics in (1-x) ZnAl<sub>2</sub>O<sub>4-x</sub>TiO<sub>2</sub> system for microwave substrate applications. *Eur Phys J B.* 2004;41:301-306.
- [24] Ohsato H, Kato K, Mizuta M, Nishigaki S, Okuda T. Microwave Dielectric Properties of the Ba<sub>6-3x</sub>(Sm<sub>1-y</sub>R<sub>y</sub>)<sub>8+2x</sub>Ti<sub>18</sub>O<sub>54</sub> (R = Nd and La) Solid Solutions with Zero Temperature Coefficient of the Resonant Frequency. *Jpn J Appl Phys.* 1995;34(9B):5413-5417.
- [25] Ball CJ, Begg BD, Cookson DJ, Thorogood GJ, Vance ER. Structures in the System CaTiO<sub>3</sub>/SrTiO<sub>3</sub>. *J Solid State Chem.* 1998;139:283-247.
- [26] Huang CH, Pana CL, Shim SJ. Liquid phase sintering of MgTiO<sub>3</sub>-CaTiO<sub>3</sub> microwave dielectric ceramics. *Mater Chem Phys.* 2003;78:111-115.
- [27] Yao GG, Liu P. Low temperature sintering and microwave dielectric properties of (1-x) Mg<sub>4</sub>Nb<sub>2</sub>O<sub>9-x</sub>CaTiO<sub>3</sub> ceramics. *Physica.* 2010;B 405:547-551.
- [28] Huang CH, Pana CL, Leeb WC. Microwave dielectric properties of mixtures of glass-forming oxides Zn-B-Si and dielectric ceramics MgTiO<sub>3</sub>-CaTiO<sub>3</sub> for LTCC applications. *J Alloys & Compounds.* 2008;462:5-8.
- [29] Cho SY, Kim IT, Hong KS. Microwave dielectric properties and applications of rare earth aluminates. *J Mater Res.* 1999;14:114-119.
- [30] Cho SY, Kim CH, Kim DW, Hongs KS, Kim JH. Dielectric properties of Ln(Mg<sub>1/2</sub>Ti<sub>1/2</sub>)O<sub>3</sub> as substrates for high-Tc superconductor thin films. *J Mater Res.* 1999;14:2484-2487.
- [31] Geller S, Bala VB. Crystallographic studies of perovskite-like compounds. II. Rare earth aluminates. *Acta Cryst.* 1956;9:1019-1025.
- [32] Inagaki Y, Suzuki S, Kagomiya I, Kakimoto K, Ohsato H, Sasaki K, Kuroda K, Shimada T. Crystal structure and microwave dielectric properties of SrTiO<sub>3</sub> doped LaAlO<sub>3</sub> single crystal grown by FZ. *J Euro Ceram Soc.* 2007;27:2861-2864.
- [33] Cho SY, Hong KS, Ko KH. Mixture-like behavior in the microwave dielectric properties of the (1-x)LaAlO<sub>3-x</sub>SrTiO<sub>3</sub> system. *Mater Res Bull.* 1999;34:511-516.
- [34] Shimada T, Kura K, Ohtsuki S. Dielectric properties and far infrared reflectivity of lanthanum aluminate-strontium titanate ceramics. *J Euro Ceram Soc.* 2006;26:2017-2021.

- [35] Inagaki Y, Ishizawa N, Ohsato H, Kagomiya I, Kakimoto K, Shimada T. Structure of Sr and Ti codoped LaAlO<sub>3</sub> perovskite. In: XXI Congress of the International Union of Crystallography Congress and General Assembly. 2008; P11.11.42(C520).
- [36] Ishizawa N, Inagaki Y, Kagomiya I, Kakimoto K, Ohsato H. Rhombohedral modification of Sr and Ti co-doped LaAlO<sub>3</sub>. Photon Factory Activity Report 2007. 2008;25(Part B):186.
- [37] Suvorov D, Valant M, Jancar B, Skapin SD. CaTiO<sub>3</sub>-based ceramics: Microstructural development and dielectric-properties. Acta Chimi Slov. 2001;48:87-99.
- [38] Galasso F, Pyle J. Ordering in compounds of the A(B<sub>0.33</sub>Ta<sub>0.67</sub>)O<sub>3</sub> type Inorg. Chem. 1963;2:482-484.
- [39] Surendran KP, Sebastian MT, Mohanan P, Moreira RL, Dias A. Effect of Nonstoichiometry on the Structure and Microwave Dielectric Properties of Ba(Mg<sub>0.33</sub>Ta<sub>0.67</sub>)O<sub>3</sub>. Chem Mater. 2005;17:142-151.
- [40] Kagata H, Kato J. Dielectric properties of Ca based complex perovskite at microwave frequencies. Jpn J Appl Phys. 1994;33:5463.
- [41] Tamura H, Konoike T, Sakabe Y, Wakino K. Microwave Dielectric Properties of Ba-Nd-Ti-O System Doped with Metal Oxides. J Am Ceram Soc. 1984;67:C-59.
- [42] Kageyama K. Research for synthesis and properties of low losses microwave dielectric ceramics [Dr. thesis]. Nagoya Institute of Technology; 1995;p. 59. (Japanese).
- [43] Seabra MP, Avdeev M, Ferreira VM, Pullar RC, Alford NMN, Reaney IM. Structure-Property Relations in  $x\text{BaTiO}_3-(1-x)\text{La}(\text{Mg}_{1/2}\text{Ti}_{1/2})\text{O}_3$  Solid Solutions. J Am Ceram Soc. 2004;87:584.
- [44] Kageyama K. Microwave dielectric properties of CaO-Ga<sub>2</sub>O<sub>3</sub>-Ta<sub>2</sub>O<sub>5</sub> ceramics. Ferroelectrics. 1990;109: 173-183.
- [45] Wakino K, Minai K, Tamura H. Formation of Self-Organized Zirconium Titanate Nanotube Layers by Alloy Anodization. J Am Ceram Soc. 1984;67:278.
- [46] Khalam LA, Sreemoolanathan H, Mohanan P, Sebastian MT. Preparation, characterization and microwave dielectric properties of Ba(B'<sub>1/2</sub> Nb<sub>1/2</sub>)O<sub>3</sub> B' = La, Pr, Nd, Sm, Eu, Gd, Tb, Dy, Ho, Y, Yb and In ceramics. Mater Sc. Engn. 2004;B107:264.
- [47] Silverman BD. Microwave Absorption in Cubic Strontium Titanate. Phys Rev. 1962;125:1921-1930.
- [48] Wakino K, Murata M, Tamura H. Far Infrared Reflection Spectra of Ba(Zn,Ta)O<sub>3</sub>-BaZrO<sub>3</sub> Dielectric Resonator Material. J Am Ceram Soc. 1986;69:34-37.
- [49] Hiuga T, Matsumoto K. Ordering of Ba(B<sub>1/3</sub>B<sub>2/3</sub>)O<sub>3</sub> Ceramics and Their Microwave Dielectric Properties. Jpn J Appl Phys. 1989;S28-2:56-58.

- [50] Kim ES, Yoon KH. Microwave Dielectric Properties of Complex Perovskite  $\text{Ba}(\text{Mg}_{1/3}\text{Ta}_{2/3})\text{O}_3$ . *Ferroelect.* 1992;133:1187.
- [51] Lu CH, Tsai CC. Reaction kinetics, sintering characteristics, and ordering behavior of microwave. *J Mater Res.* 1996;11:1219-1227.
- [52] Kawashima S, Nishida M, Ueda I, Ouchi H.  $\text{Ba}(\text{Zn}_{1/3}\text{Ta}_{2/3})\text{O}_3$  Ceramics with Low Dielectric Loss at Microwave Frequencies. *J Am Ceram Soc.* 1983;66:421-423.
- [53] Yokotani Y, Tsuruta T, Okuyama K, Kugimiya K. Low-Dielectric Loss Ceramics for Microwave Uses. National Technical Report. 1994;40:11-16. (Japanese).
- [54] Matsumoto H, Tamura H, Wakino K.  $\text{Ba}(\text{Mg}, \text{Ta})\text{O}_3$ - $\text{BaSnO}_3$  High-Q Dielectric Resonator. *Jpn J Appl Phys.* 1991;30:2347-2349.
- [55] Koga E, Moriwake H. Effects of Superlattice Ordering and Ceramic Microstructure on the Microwave  $Q$  Factor of Complex Perovskite-Type Oxide  $\text{Ba}(\text{Zn}_{1/3}\text{Ta}_{2/3})\text{O}_3$ . *J Ceram Soc Jpn.* 2003;111:767-775 (Japanese).
- [56] Koga E, Moriwake H, Kakimoto K, Ohsato H. Influence of Composition Deviation from Stoichiometric  $\text{Ba}(\text{Zn}_{1/3}\text{Ta}_{2/3})\text{O}_3$  on Superlattice Ordering and Microwave Quality Factor  $Q$ . *J Ceram Soc Jpn.* 2005;113: 172-178 (Japanese).
- [57] Koga E, Mori H, Kakimoto K, Ohsato H. Synthesis of Disordered  $\text{Ba}(\text{Zn}_{1/3}\text{Ta}_{2/3})\text{O}_3$  by Spark Plasma Sintering and Its Microwave  $Q$  Factor. *Jpn J Appl Phys.* 2006;45(9B): 7484-7488.
- [58] Koga E, Yamagishi Y, Moriwake H, Kakimoto K, Ohsato H. Order-disorder transition and its effect on Microwave quality factor  $Q$  in  $\text{Ba}(\text{Zn}_{1/3}\text{Nb}_{2/3})\text{O}_3$  system. *J Electroceram.* 2006;17:375-379.
- [59] Koga E, Yamagishi Y, Moriwake H, Kakimoto K, Ohsato H. Large  $Q$  factor variation within dense, highly ordered  $\text{Ba}(\text{Zn}_{1/3}\text{Ta}_{2/3})\text{O}_3$  system. *J Euro Ceram Soc.* 2006;26:1961-1964.
- [60] Kugimiya K. Crystallographic study on the  $Q$  of  $\text{Ba}(\text{Mg}_{1/3}\text{Ta}_{2/3})\text{O}_3$  dielectrics. In: Abstract for Kansai branch academic meeting. 5 September 2003; Senri-Life Science. B-20. In: Abstract for Meeting of Microwave/Millimeterwave Dielectrics and Related Materials on the Ceramic Soc. 2004; Nagoya Institute of Technology: Nagoya Japan. (Japanese).
- [61] Surendran KP, Sebastian MT, Mohanan P, Moreira RL, Dias A. Effect of Nonstoichiometry on the Structure and Microwave Dielectric Properties of  $\text{Ba}(\text{Mg}_{0.33}\text{Ta}_{0.67})\text{O}_3$ . *Chem Mater.* 2005;17:142-151.
- [62] Koga E, Moriwake H, Kakimoto K, Ohsato H. Raman Spectroscopic Evaluation and Microwave Dielectric Property of Order/Disorder and Stoichiometric/Non-Stoichiometric  $\text{Ba}(\text{Zn}_{1/3}\text{Ta}_{2/3})\text{O}_3$ . *Ferroelectrics.* 2007;356:146-152.

- [63] Izumi F, Ikeda T. A Rietveld-analysis program RIETAN-98 and its applications to zeolites. *Mater Sci Forum*. January 2000;321-324:198-203.
- [64] Kolodiaznyi T. Origin of extrinsic dielectric loss in 1:2 ordered, single-phase  $\text{BaMg}_{1/3}\text{Ta}_{2/3}\text{O}_3$ . *J Euro Ceram Soc*. 2014;34:1741-1753.
- [65] Ohsato H, Koga E, Kagomiya I, Kakimoto K. Origin of High Q for Microwave Complex Perovskite. *Key Eng Mat*. 2010;421-422:pp77-80.
- [66] Ohsato H, Koga E, Kagomiya I, Kakimoto K. Phase Relationship and Microwave Dielectric Properties in the Vicinity of  $\text{Ba}(\text{Zn}_{1/3}\text{Ta}_{2/3})\text{O}_3$ . *Ceram Eng & Sci Proc*. 2010;30:25-35.
- [67] Ohsato H, Koga E, Kagomiya I, Kakimoto K. Dense Composition with High-Q on the Complex Perovskite Compounds. *Ferroelectrics*. 2009;387:28-35.
- [68] Roth RS, Beach F, Antoro A, Davis K, Soubeyroux JL. Structural of the nonstoichiometric solid solutions  $\text{Ba}_2\text{RE}_4[\text{Ba}_x\text{RE}_{2/3-2/3x}]\text{Ti}_9\text{O}_{27}$  (RE = Nd, Sm). In:14 Int Congress Crystallog: Collected Abst; 1987; Perth: Australia; 07. 9-9.
- [69] Ohsato H, Ohhashi T, Nishigaki S, Okuda T, Sumiya K, Suzuki S. Formation of solid solution of new tungsten bronze-type microwave dielectric compounds  $\text{Ba}_{6-3x}\text{R}_{8+2x}\text{Ti}_{18}\text{O}_{54}$  (R = Nd and Sm,  $0 \leq x \leq 1$ ). *Jpn J Appl Phys*. 1993;32:4323-4326.
- [70] Matveeva, RG, Varforomeev MB, Il'yuschenko LS. Refinement of the composition crystal structure of  $\text{Ba}_{3.75}\text{Pr}_{9.5}\text{Ti}_{18}\text{O}_{54}$ . *Zh Neorg Khim*. 1984;29:31-34 (Trans. Russ: J Inorg Chem. 1984;29:17-19).
- [71] Ohsato H, Ohhashi T, Okuda T. Structure of  $\text{Ba}_{6-3x}\text{Sm}_{8+2x}\text{Ti}_{18}\text{O}_{54}$  ( $0 < x < 1$ ). In Ext. Abstr. AsCA '92 Conf; November 1992; Singapore: 14U-50.
- [72] Ohsato H. Science of tungstenbronze-type like  $\text{Ba}_{6-3x}\text{R}_{8+2x}\text{Ti}_{18}\text{O}_{54}$  (R= rare earth) microwave dielectric solid solutions. *J Euro Ceram Soc*. 2001;21:2703-2711.
- [73] Ohsato H, Nishigaki S, Okuda T. Superlattice and dielectric properties of dielectric compounds. *Jpn J Appl Phys*. 1992;31(9B):3136-3138.
- [74] Ohsato H, Imaeda M, Takagi Y, Komura A, Okuda T. Microwave quality factor improved by ordering of Ba and rare-earth on the tungstenbronze-type  $\text{Ba}_{6-3x}\text{R}_{8+2x}\text{Ti}_{18}\text{O}_{54}$  (R = La, Nd and Sm) Solid Solutions. In Proceeding of the XIth IEEE International Symposium on Applications of Ferroelectrics. IEEE catalog number 98CH36245; 1998: p. 509-512.
- [75] Ohsato H, Mizuta M, Ikoma T, Onogi Z, Nishigaki S, Okuda T. Microwave Dielectric Properties of Tungsten Bronze-Type  $\text{Ba}_{6-3x}\text{R}_{8+2x}\text{Ti}_{18}\text{O}_{54}$  (R = La, Pr, Nd and Sm) Solid Solutions. *J Ceram Soc Jpn. Int Edition*. 1998;106-185:184-188.
- [76] Ohsato H, Mizuta M, Okuda T. Crystal Structure and Microwave Dielectric Properties of Tungstenbronze-type  $\text{Ba}_{6-3x}\text{R}_{8+2x}\text{Ti}_{18}\text{O}_{54}$  (R = La, Nd and Sm) Solid Solutions. In:

- Morawiec H, Stroz D, editors. *Applied Crystallography*. World Scientific Publishing; 1998: p. 440-447.
- [77] Ohsato H, Imaeda M, Komura A, Okuda T. Non-Linear Microwave Quality Factor Change Based on the Site Occupancy of Cations on the Tungstenbronze-type  $\text{Ba}_{6-3x}\text{R}_{8+2x}\text{Ti}_{18}\text{O}_{54}$  ( $R = \text{Rare Earth}$ ) Solid Solutions. In: K. M. Nair KM, Bhalla AS, editors. *Dielectric Ceramic Materials*. In: *Ceramic Transaction*. John Wiley & Sons; 1998;100:p41-50.
- [78] Valant M, Sovorov D, Kolar D. X-Ray Investigations and Determination of Dielectric Properties of the Compound  $\text{Ba}_{4.5}\text{Gd}_9\text{Ti}_{18}\text{O}_{54}$ . *Jpn J Appl Phys*. 1996;35:144-150.
- [79] Shannon RD. Dielectric polarizabilities of ions in oxides and fluorides. *J Appl Phys*. 1993;73:348.
- [80] Ohsato H, Sugino J, Komura A, Nishigaki S, Okuda T. Microwave Dielectric Properties of  $\text{Ba}_4(\text{Nd}_{2/3-y}\text{R}_y)\text{Ti}_{18}\text{O}_{54}$  ( $R = \text{Eu, Dy, Ho, Er and Yb}$ ) Solid Solutions. *Jpn J Appl Phys*. 1999;38(9B):5625-5628.
- [81] Ohsato H. *Crystallography and R&D for Material Science from Our Research: Electroceramics*. *Advanced Materials Research*. 2006;11-12:95-100.
- [82] Nagatomo T, Otagiri T, Suzuki M, Ohsato H. Microwave dielectric properties and crystal structure of the tungstenbronze-type like  $(\text{Ba}_{1-\alpha}\text{Sr}_\alpha)_6(\text{Nd}_{1-\beta}\text{Y}_\beta)_8\text{Ti}_{18}\text{O}_{54}$  solid solutions. *J Eur Ceram Soc*. 2006;26:1895-1898.
- [83] Suzuki M, Ohsato H, Kakimoto K, Nagatomo T, Otagiri T. Crystal structure and microwave dielectric properties of  $(\text{Ba}_{1-\alpha}\text{Sr}_\alpha)_{6-3x}\text{Sm}_{8+2x}\text{Ti}_{18}\text{O}_{54}$  solid solutions. *J Eur Ceram Soc*. 2006;26:2035-2038.
- [84] Mercurio D, Abou-Salama M, Mercurio PJ, Investigations of the Tungsten-bronze-Type  $(\text{Ba}_{1-\alpha}\text{Sr}_\alpha)_{6-x}\text{La}_{8+2x/3}\text{Ti}_{18}\text{O}_{54}$  ( $0 = x = 3$ ) Solid Solutions. *J Eur Ceram Soc*. 2001;21:2713-2716.
- [85] Imaeda M, Ito K, Mizuta M, Ohsato H, Nishigaki S, Okuda T. Microwave dielectric properties of  $\text{Ba}_{6-3x}\text{Sm}_{8+2x}\text{Ti}_{18}\text{O}_{54}$  solid solutions with Sr substituted for Ba. *Jpn J Appl Phys*. 1997;36(9B):6012-6015.
- [86] Ohsato H, Suzuki M, Kakimoto K. Ionic Distribution and Microwave Dielectric Properties for Tungstenbronze-Type Like  $\text{Ba}_{6-3x}\text{R}_{8+2x}\text{Ti}_{18}\text{O}_{54}$  ( $R = \text{Sm, Nd and La}$ ) Solid Solutions. *Ceramic Engineering and Science Proceedings*. 2005;26(5):135-145.
- [87] Ishizawa N. Layered Perovskite-Structural Classification. *Ceramics*. 1996;31:409-413 (Japanese).
- [88] Magnéli A. Structures of the  $\text{ReO}_3$ -type with recurrent dislocations of atoms: 'homologous series' of molybdenum and tungsten oxides. *Acta Cryst*. 1953;6:495-500. DOI: 10.1107/S0365110X53001381

- [89] Trolliard G, Harre N, Mercurio D, Frit B. Cation-deficient perovskite-related  $(\text{Ba, La})_n\text{Ti}_{n-\delta}\text{O}_{3n}$  ( $n \geq 4\delta$ ) microphases in the  $\text{La}_4\text{Ti}_3\text{O}_{12}$ - $\text{BaTiO}_3$  system: An HRTEM approach. *J Solid State Chem.* 1999;145:678-693.
- [90] Teneze N, Mercurio D, Trolliard G, Frit B. Cation-deficient perovskite-related compounds  $(\text{Ba, La})_n\text{Ti}_{n-1}\text{O}_{3n}$  ( $n = 4, 5, \text{ and } 6$ ): Rietveld refinement from neutron powder diffraction data. *Mater Res Bull.* 2000;35:1603-1614.
- [91] Harre N, Mercurio D, Trolliard G, Frit B. Crystal structure of  $\text{BaLa}_4\text{Ti}_4\text{O}_{15}$ , member  $n=5$  of the homologous series  $(\text{Ba, La})_n\text{Ti}_{n-1}\text{O}_{3n}$  of cation-deficient perovskite-related compounds. *Mater Res Bull.* 1998;33:1537-1548.
- [92] Harre N, Mercurio D, Trolliard G, Frit B. Crystal structure of  $\text{BaLa}_4\text{Ti}_5\text{O}_{15}$  member  $n=6$  of the homologous series  $(\text{Ba, La})_n\text{Ti}_{n-1}\text{O}_{3n}$  of cation deficient perovskite related compounds. *J Solid State Inorg. Chem.* 1998;35:77.
- [93] Okawa T, Kiuchi K, Okabe H, Ohsato H. Microwave dielectric properties of  $\text{Ba}_n\text{La}_4\text{Ti}_{3+n}\text{O}_{12+3n}$  Homologous Series. *Jpn J Appl Phys.* 2001;40:5779-5782.
- [94] Okawa T, Kiuchi K, Ohsato H. Microwave dielectric properties of  $\text{Ba}_n\text{La}_4\text{Ti}_{3+n}\text{O}_{12+3n}$  Homologous Compounds and Substitution of Trivalent Cations for La. *Ferroelectrics.* 2002;272:345-350.
- [95] Ohsato H, Tohdo Y, Kakimoto K, Okabe H, Okawa T. Crystal structure and microwave dielectric properties of  $\text{BaLa}_4\text{Ti}_{3+n}\text{O}_{12+3n}$  homologous compounds with high dielectric constant and high quality factor. *Ceramic Engineering and science Proceedings.* 2003;24:75-80.
- [96] Tohdo Y, Kakimoto K, Ohsato H, Okawa T and Okabe H. Crystal Structure Analysis of Homologous Compounds  $\text{ALa}_4\text{Ti}_4\text{O}_{15}$  ( $A=\text{Ba, Sr and Ca}$ ) and their Microwave Dielectric Properties. *Ceramic Engineering and Science Proceedings.* 2005;26:147-153.
- [97] Tohdo Y, Kakimoto K, Ohsato H, Yamada H, Okawa T. Microwave dielectric properties and crystal structure of homologous compounds  $\text{ALa}_4\text{Ti}_4\text{O}_{15}$  ( $A = \text{Ba, Sr and Ca}$ ) for base station applications. *J Eur Ceram Soc.* 2006;26:2039-2043.
- [98] Ruddlesden SN, Popper P. New compounds of the  $\text{K}_2\text{NIF}_4$  type. *Acta Cryst.* 1957;10:538-539. DOI: 10.1107/S0365110X57001929
- [99] Ruddlesden SN, Popper P. The compound  $\text{Sr}_3\text{Ti}_2\text{O}_7$  and its structure. *Acta Cryst.* 1958;11:54-55. DOI: 10.1107/S0365110X58000128
- [100] Fan XC, Chen XM. Microstructure and Microwave Dielectric Properties of the  $\text{CaSmAlO}_4$ -Based Ceramics. *J Am Ceram Soc.* 2008;91:2917-22.
- [101] Aurivillius B. Mixed bismuth oxides with layer lattices II. Structure of  $\text{Bi}_4\text{Ti}_3\text{O}_{12}$ . *Arkiv Kemi.* 1949;1:499.
- [102] Galasso FS. *Structure and Properties of Inorganic Solids.* New York: Pergamon Press; 1970. 308 p.

- [103] Dion M, Ganne M, Tournoux M. Nouvelles familles de phases  $M^I M^{II}_2 Nb_3 O_{10}$  a feuillets "perovskites". *Mater Res Bull.* 1981;16:1429-1435.
- [104] Jacobson AJ, Johnson JW, Lewandowski JT. Interlayer chemistry between thick transition-metal oxide layers: synthesis and intercalation reactions of  $K[Ca_2 Na_{n-3} Nb_n O_{3n+1}]$  (3.ltoreq. n.ltoreq. 7). *Inorg Chem.* 1985;24:3727-3729.
- [105] Ishizawa N, Marumo F, Kawamura T, Kimura M. Compounds with perovskite-type slabs. II. The crystal structure of  $Sr_2 Ta_2 O_7$ . *Acta Cryst.* 1976;B32:2564-2566.
- [106] Ishizawa N, Marumo F, Iwai S. Compounds with perovskite-type slabs. IV. Ferroelectric phase transitions in  $Sr_2(Ta_{1-x} Nb_x)_2 O_7$  ( $x$  0.12) and  $Sr_2 Ta_2 O_7$ . *Acta Cryst.* 1981;B37:26-31.
- [107] Nanot PM, Queyroux F, Gilles JC, Chevalier R. Structure cristalline du composé  $Nd_4 Ca_2 Ti_6 O_{20}$ , terme  $n=6$  de la série  $(Nd, Ca)_n, Ti_n O_{3n+2}$ . *Acta Cryst.* 1976; B32: 1115-1120.
- [108] Okawa T. Research for  $BaO-R_2 O_3-TiO_2$  ( $R$  = Rear Earth) microwave dielectric ceramics [Dr. thesis]. Nagoya Institute of Technology; 2003. (Japanese)
- [109] Valant M, Suvorov D, Kolar D. Role of  $Bi_2 O_3$  in optimizing the dielectric properties of  $Ba_{4.5} Nd_9 Ti_{18} O_{54}$  based microwave ceramics. *J Mat Res.* 1996;11:928-931.
- [110] Okawa T, Imaeda M, Ohsato H. Microwave Dielectric Properties of Bi-Added  $Ba_4 Nd_{9+1/3} Ti_{18} O_{54}$  Solid Solutions. *Jpn J Appl Phys.* 2000;39(9B):5645-5649.
- [111] Yamada H, Okawa T, Tohdo Y, Ohsato H. Microwave dielectric properties of  $Ba_x La_4 Ti_{3+x} O_{12+3x}$  ( $x = 0.0-1.0$ ) ceramics. *J Eur Ceram Soc.* 2006;26:2059-2062.
- [112] Ohsato H, Harada A, Okawa T, Okabe H. Microwave dielectric composite composition. US 7,046,258 B2, (2006).
- [113] Murakami M, Hirose K, Kawamura K, Sata N, Ohishi Y. Post-perovskite phase transition in  $MgSiO_3$ . *Science.* 2004;304:855-858.
- [114] Lundberg M, Sundberg M, Magneli A. The "Pentagonal Column" as a Building Unit in Crystal and Defect Structure of Some Groups of Transition Metal Compounds. *J Solid State Chem.* 1982;44:32-40.
- [115] Ohsato H. Functional advances of microwave dielectrics for next generation. *Ceramics International*, 2012;38S:S141-S146.
- [116] Tenue Publicity Group. Grain 29: TV ghost hunted/effect of natural resonating/electromagnetic-wave absorption. In: A guidebook of micro cosmos for ferrite/With ferrite. TDK Corporation; 2007: p. 86-87. (Japanese)
- [117] Tanaka N. High refractive transparency ceramics. *FC Report.* 2003;21:90-91. (Japanese).